Synthesis, Characterization, and Reactivity of a (PPP) Pincer-Ligated Manganese Carbonyl Complex: Polarity Reversal Imparted by the Electrophilic Nature of a Planar Mn-P(NR_2)$_2$ Fragment

Leah K. Oliemuller, Curtis E. Moore, Christine M. Thomas*

Department of Chemistry and Biochemistry, The Ohio State University, 100 West 18th Avenue, Columbus, Ohio 43210, United States

Supporting Information Placeholder

ABSTRACT: The bonding interactions of a synthesized pincer-ligated manganese dicarbonyl complex featuring an N-heterocyclic phosphenium (NHP^+) central moiety are explored. The pincer ligand [PPP]Cl was coordinated to a manganese center using $Mn(CO)_5Br$ and 254 nm light to afford the chlorophosphine complex ($PP^{Cl}P$)$Mn(CO)_2Br$ (**2**) as mixture of halide exchange products and stereoisomers. The target dicarbonyl species (PPP)$Mn(CO)_2$ (**3**) was prepared by treatment of **2** with two equivalents of the reductant KC_8. Computational investigations and analysis of structural parameters were used to elucidate multiple bonding interactions between the Mn center and the P^{NHP} atom in **3**. The generation of a product of formal H_2 addition, ($PP^{H}P$)$Mn(CO)_2H$ (**4**), was achieved through the dehydrogenation of NH_3BH_3, affording a 2:1 mixture of $\mathbf{4}^{\mathbf{syn}}$:$\mathbf{4}^{\mathbf{anti}}$ stereoisomers. The nucleophilic nature of the Mn center and the electrophilic nature of the P^{NHP} moiety were demonstrated through hydride addition and protonation of **3** to produce $K(THF)_2$[($PP^{H}P$)$Mn(CO)_2$] (**6**) and ($PP^{Cl}P$)$Mn(CO)_2H$ (**5**), respectively. The observed reactivity suggests that **3** is best described as a Mn^{-I}/NHP^+ complex, in contrast to pincer-ligated dicarbonyl manganese analogues typically assigned as Mn^{I} species.

INTRODUCTION

Tremendous progress has been made in recent years toward the development of base metal catalysts, as both economic and environmental pressures have limited the sustained use of noble metals in homogeneous catalysis.[1–5] To this end, much attention has been paid to employing Earth-abundant manganese in transition metal complexes with applications in small molecule activation and catalysis.[6,7] In particular, pincer-ligated manganese complexes have been used as dehydrogenation and hydrogenation catalysts to achieve a variety of chemical transformations,[6–8] with some notable examples including dehydrogenative coupling reactions to afford industrially relevant building blocks like imines,[9,10] amides,[11] and N-heterocycles such as pyrroles and pyrimidines,[12–16] the reduction of CO_2,[17–20] and H-E (E = B, P, Si) hydroelementation reactions.[8] The coordination of a pincer ligand scaffold to these transition metal catalysts has been popularized to impart stability in well-defined structures through chelation as well as provide steric and electronic tunability via selection and modification of the coordinating groups and backbone linkers.[21]

The first examples of pincer-ligated manganese carbonyl complexes with utility in catalytic hydrogenation and dehydrogenation were reported as recently as 2016,[6–8] pioneered by the groups of Milstein, Beller, Kirchner, Liu, and Kempe (Chart 1).[9,10,22–25] These complexes feature non-innocent tridentate ligands and utilize metal-ligand cooperativity to promote more facile bond activation using first-row transition metals, which are generally more challenging to achieve than when using noble metals.[26,27] Typically, these manganese complexes are supported by PNP or NNP pincer ligands and proceed through the dearomatization of the pincer ligand's linkers or deprotonation of a nitrogen moiety to generate a vacant site for the addition of small molecules. This

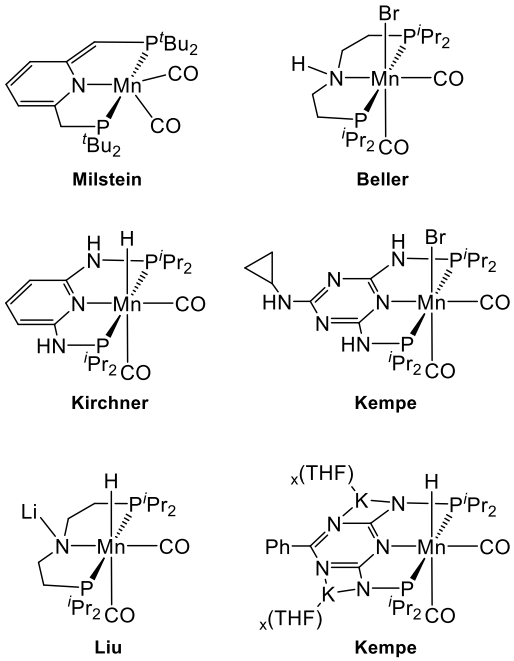

Chart 1. Examples of selected pincer-ligated manganese carbonyl hydrogenation/dehydrogenation catalysts/precatalysts.[9,10,22–25]

cooperative formula using pincer ligands remains an active area of study and has expanded the breadth of hydrogenation to more challenging substrates.[8] However, the isolable and characterized species in these catalytic processes are often the precatalysts (**I**), which require the addition of base to access the proposed coordinatively unsaturated catalytic species (**II**) via deprotonation of the non-innocent ligand and removal of a halide, as shown in a general hydrogenation catalytic cycle in Figure 1. In addition to requiring excess base, many of these catalytic processes require very harsh conditions using high pressures of H_2 (up to 80 bar) and high temperatures (> 100 °C) to cleave H_2 across the M-L bond (**III**).[7] Often times, intermediates like **II** or **III** within the catalytic cycle are only observed *in situ* and not isolable. Isolation of such species could allow for studies of metal-ligand cooperative H_2 addition and provide further insight toward base metal catalyst design using milder conditions.

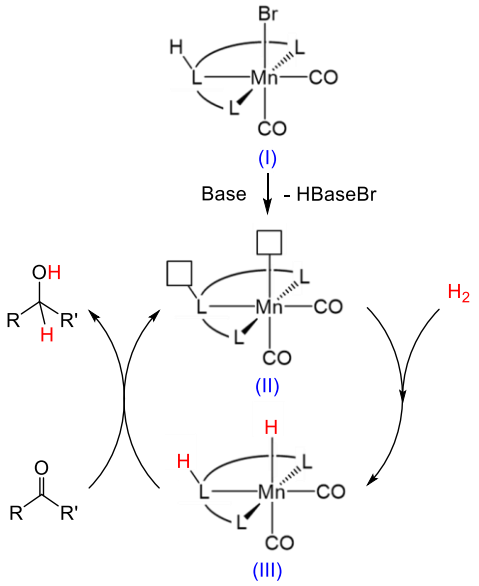

Figure 1. General metal-ligand cooperative catalytic cycle using pincer-ligated manganese carbonyl complexes for the hydrogenation of ketones or aldehydes.

Far less attention has been paid toward reactivity across manganese-phosphorus bonds, particularly when the phosphorus atom is incorporated into an N-heterocycle, for these hydrogenation/dehydrogenation processes.[28–31] Gudat and coworkers demonstrated the catalytic dehydrogenation of ammonia borane across a Mn-P bond using a manganese carbonyl complex featuring a monodentate N-heterocyclic phosphenium (NHP^+) ligand (Chart 2).[30] In this monodentate (^{Dipp}NHP)Mn(CO)$_4$ (Dipp = 2,6-diisopropylphenyl) system, an electrophilic phosphenium ligand provides a Lewis acidic reaction center to promote this transformation and is the first example of a terminal N-heterocyclic phosphenium complex applied in catalysis. Our group has previously demonstrated E-H (E = H, B, O, S) bond activations across M-P^{NHP} bonds using a variety of late transition metals coordinated by a non-innocent PPP pincer ligand featuring an N-heterocyclic phosphenium/phosphido ($NHP^{+/-}$) moiety in the central position.[32–38] For example, the Co^I N-heterocyclic phosphido (NHP^-) complex (PPP)Co(PMe$_3$) was reported to undergo the first example of H_2 activation involving metal-ligand cooperativity between any first-row metal and a phosphorus atom (Chart 2).[34] The $NHP^{+/-}$ moiety allows for the possibility of polarity reversal of the M-P^{NHP} bond,[39] which may lead to alternative metal-ligand cooperative pathways that differ from those explored by the traditionally employed PNP ligand systems shown in Chart 1.

In this study, we seek to explore the reactivity across a Mn-P^{NHP} bond when using a less-electron rich earlier metal compared to our previous library of late transition metal complexes and an $NHP^{+/-}$ unit supported by a chelating pincer ligand framework. We aim to gain further insight into key fundamental steps in heterolytic H_2 cleavage reactions by studying isolable, well-defined dicarbonyl Mn species with the potential for polarity reversal of the metal-ligand bond provided by a non-innocent $NHP^{+/-}$ ligand. Herein, we describe the synthesis and characterization of a coordinatively unsaturated pincer-ligated manganese carbonyl complex and assess the nature of the Mn-P^{NHP} bonding interaction using both computational investigations and reactivity studies toward H^+/H^- for future applications.

Chart 2. A Lewis acidic NHP^+ center used in the dehydrogenation of NH_3BH_3 by Gudat et al. (top) and the metal-ligand cooperative activation of H_2 using a nucleophilic NHP^- ligand by Thomas et al. (bottom).[30,34]

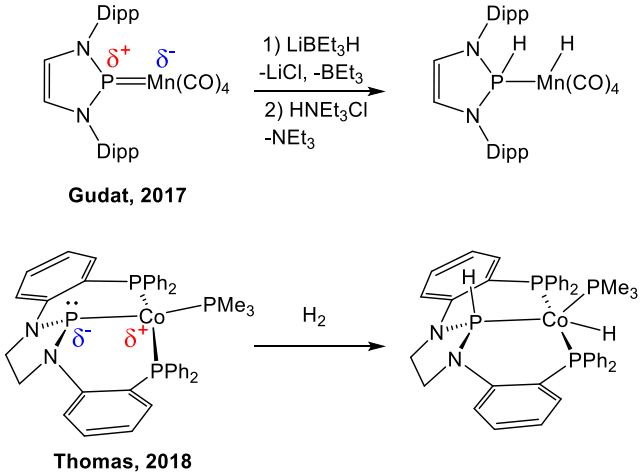

RESULTS AND DISCUSSION

Coordination of [PPP]Cl to Manganese. To coordinate our ligand scaffold to a manganese center, the previously reported chlorophosphine ligand precursor [PPP]Cl (**1**)[32] was added to the Mn^I precursor Mn(CO)$_5$Br and irradiated with 254 nm light (Scheme 1). The $^{31}P\{^1H\}$ NMR spectrum of this reaction on a scale of 40 mg of **1** and 30 mL total of THF features a triplet at 181.4 ppm and a doublet at 51.9 ppm (Figure S2). These signals integrate in a 1:2 ratio and correspond to the halide-bonded NHP phosphorus center and two chemically equivalent diarylphosphine sidearms, respectively, of the resulting chlorophosphine complex ($PP^{Cl}P$)Mn(CO)$_2$Br (**2**). Single-crystal X-ray diffraction confirmed the identity of **2** as an octahedral Mn^I complex in which the bromide ligand is located trans to the central NHP phosphorus atom and the carbonyl ligands are mutually trans (Figure 2). Crystallographic refinement revealed significant disorder resulting from exchange of the Br^- and Cl^- ligands between the P-bound and Mn-bound positions of **2**, such that 82% of the molecules in the structure are ($PP^{Cl}P$)Mn(CO)$_2$Br (**2**) and 18% are ($PP^{Br}P$)Mn(CO)$_2$Cl (**2***). Evidence for halide exchange during the synthesis **2** is also evident from the small additional $^{31}P\{^1H\}$ NMR resonances in samples of **2** prepared under these conditions (Figure S2, *vide infra*).

The coordination of comparable tridentate ligands to $Mn(CO)_5Br$ are typically achieved using heat.[22,23,40] However, the reaction of **1** with $Mn(CO)_5Br$ refluxing in toluene at 130 °C results in a reaction mixture containing multiple products, none of which correspond to **2**, and most of which are likely accredited to ligand decomposition due to their significantly upfield chemical shifts (ca. -20 ppm) (Figure S7). We posit that irradiation with UV light is required to dissociate three carbonyl ligands from the metal center to allow for the coordination of the tridentate ligand.

Scheme 1. Synthesis of $(PP^{Cl}P)Mn(CO)_2Br$ Using UV Light

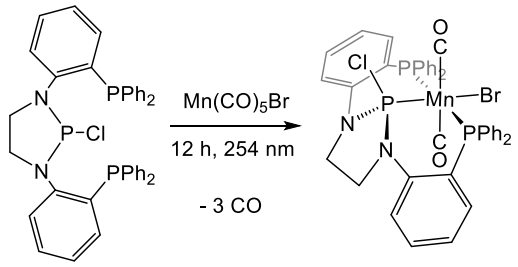

1 **2**

In addition to temperature sensitivity, the formation of **2** appears to be highly dependent on both reaction scale and volume of solvent used. A larger scale reaction of **1** (>100 mg) and $Mn(CO)_5Br$ in 30 mL of THF affords a mixture of at least five products each with two $^{31}P\{^1H\}$ NMR resonances in a 1:2 integral ratio at chemical shifts very similar to **2**, as well as the growth of several impurities at 259 and -17 ppm that are likely attributed to the formation of dimeric species and dissociated ligand, respectively (Figure S8). Although this reaction was previously shown to proceed relatively cleanly on a smaller scale while using 30 mL THF, both doubling the concentration of **1** or doubling the volume of THF used greatly increases the number and proportion of similar byproducts formed and introduces new impurities (Figure S9).

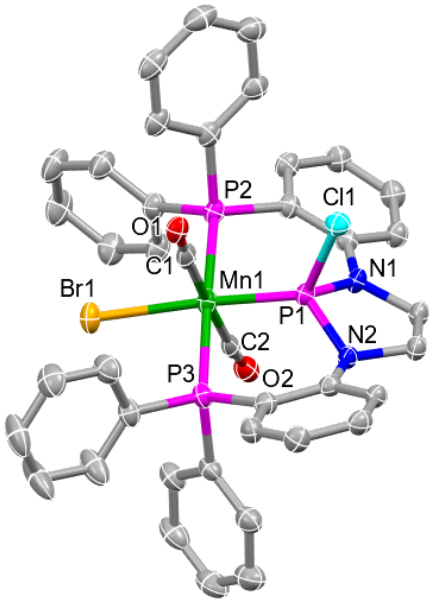

Figure 2. Displacement ellipsoid (50%) representation of **2**. Refinement revealed significant disorder resulting from exchange of the Cl^- and Br^- ligands between the P- and Mn-bound positions (82% $(PP^{Cl}P)Mn(CO)_2Br$ (**2**)/18% $(PP^{Br}P)Mn(CO)_2Cl$ (**2***)). All hydrogen atoms, Cl1B and Br1B of the minor component **2***, and solvate molecule have been omitted for clarity. Relevant bond distances (Å) and angles (°): Mn1-P1, 2.0918(7); Mn1-P2, 2.2752(7); Mn1-P3, 2.2930(7); P1-Mn1-Br1, 175.32(6); P2-Mn1-P3, 176.28(3); C1-Mn1-C2, 178.08(11).

The aforementioned disordered halide positions in the solid-state structure of **2**, combined with the similarity of $^{31}P\{^1H\}$ NMR resonances of **2** and the byproducts formed under different conditions led us to believe that halide exchange could be accounting for some of the additional products in the mixture. To support this hypothesis, the bromide-containing analogue of **1**, [PPP]Br (**1-Br**), was synthesized according to literature procedure,[32] and an analogue of **2** where both halides are bromides, $(PP^{Br}P)Mn(CO)_2Br$, was prepared using the same procedure for the synthesis of **2** using **1-Br** in place of **1**. The resulting $^{31}P\{^1H\}$ NMR spectrum features one main product with central NHP phosphorus and diarylphosphine sidearm resonances at 174.2 and 52.9 ppm, respectively, and accounts for a minor product with the same chemical shifts observed in the $^{31}P\{^1H\}$ spectrum when using chloride-containing **1** (Figures S10-S11). However, two small phosphine sidearm doublets at 58.6 and 56.9 ppm are observed in the $^{31}P\{^1H\}$ NMR spectrum of $(PP^{Br}P)Mn(CO)_2Br$, suggesting that stereoisomerism of the metal-bound halide may be occurring in combination with halide exchange processes to manifest the additional products in the mixture.

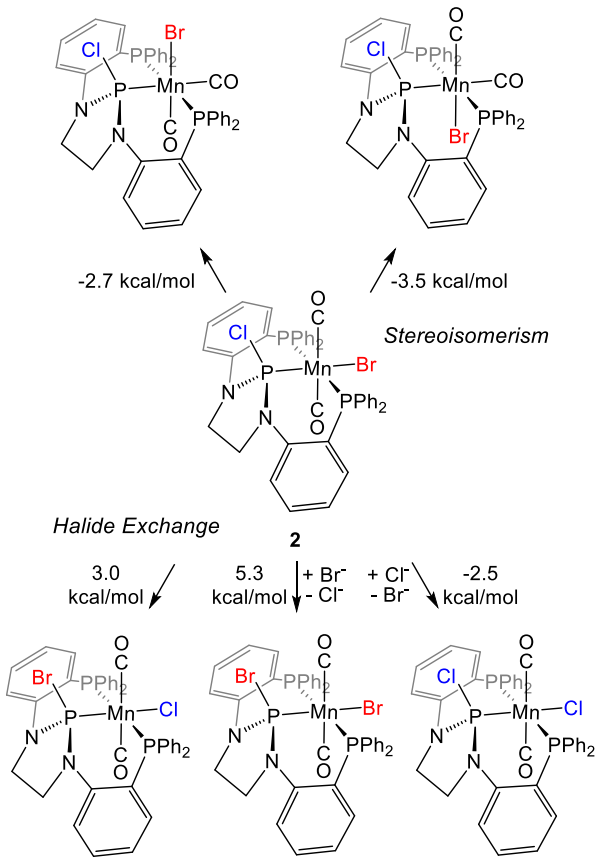

Figure 3. Relative calculated free energies of **2**, (top) stereoisomers of **2**, and (bottom) halide exchange analogues of **2**.

Computational studies were performed using density functional theory (DFT) to support the energetic feasibility of these isomers. Geometry optimizations were carried out starting from

the crystallographically derived Cartesian coordinates of **2**, and the computed bond metrics agreed with those observed using X-ray crystallography (Table S3). The halide atoms and CO ligands in the crystal structure of **2** were then modified to constitute each of the halide exchange analogues and stereoisomers and optimized once more (Tables S4-S8). Frequency calculations (Table S10) reveal that the difference in free energies of the proposed byproducts and **2** are all within 5 kcal/mol (Figure 3), suggesting that the additional products in reactions between **1** and $Mn(CO)_5Br$ observed under different conditions are likely ascribed to halide exchange and/or stereoisomerism.

Furthermore, elemental analysis data were collected using pure samples of **2** and samples obtained from largescale reactions between **1** and $Mn(CO)_5Br$ under photolysis conditions, with the assumption that the CHN constitution of a mixture of halide exchange products and stereoisomers should be identical to that of **2**. Indeed, the CHN percentages of the mixture of products (C, 56.63; H, 3.89; N, 3.11) were like those of **2** (C, 56.84; H, 4.09; N, 3.23), and in agreement with the calculated values (C, 57.47; H, 3.86; N, 3.35). Taken together, the elemental analysis data, the similarity in $^{31}P\{^1H\}$ NMR spectra, the crystallographic disorder in the halide positions of **2**, the assignment of at least one minor product of the mixture to $(PP^{Br}P)Mn(CO)_2Br$ via independent synthesis, and the small calculated differences in free energy of various isomers supports our hypothesis that the mixture of products observed in the synthesis of **2** is owed to fluxional processes that give rise to halide exchange products and/or cis/trans stereoisomers.

Synthesis and Characterization of $(PPP)Mn(CO)_2$. Despite the formation of a mixture of similar products in the synthesis of **2**, we proceeded to pursue our target complex, $(PPP)Mn(CO)_2$ (**3**), since both halides are ultimately removed. A mixture containing complex **2** and its isomers was treated with two equivalents of KC_8 to remove both halides as potassium salts and formally reduce the Mn^I center to afford the Mn^I complex **3** (Scheme 2). Cyclic voltammetry measurements of **2** reveal two irreversible reductions at very negative potentials (-2.51 and -2.83 V vs ferrocene) (Figures S63-S66). The irreversibility of these reductions is consistent with chemical transformations corresponding to the loss of each halide from **2**.

Scheme 2. Reduction of $(PP^{Cl}P)Mn(CO)_2Br$ to $(PPP)Mn(CO)_2$

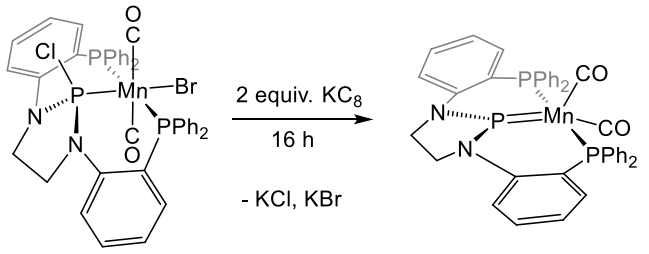

2 **3**

The $^{31}P\{^1H\}$ NMR spectrum of **3** shows one single product with corresponding NHP phosphorus atom and phosphine sidearm resonances at 203.8 (triplet) and 67.0 ppm (doublet), respectively. The downfield-shifted (vs 181.4 ppm in **2**) central phosphorus atom resonance is indicative of the successful removal of the halide on the central NHP phosphorus atom.[41] In addition, the convergence to one product from the mixture of isomers of **2** with similar chemical shifts further supports the assignment of the byproducts as stereoisomers or halide exchange products of **2**. The ^1H NMR spectrum of **3** features just one aliphatic resonance at 3.94 ppm assigned to the four protons on the heterocycle's carbon backbone, consistent with an increase in symmetry compared to **2**.

The structure of complex **3** in the solid state was confirmed using single-crystal X-ray diffraction (Figure 4). The solid-state structure reveals Mn-P bond distances of 2.2362(5) and 2.2206(5) Å to each of the diarylphosphine sidearms, typical compared to those observed in other Mn-P σ-donation interactions.[10,23,42] However, the Mn-P bond distance to the central NHP phosphorus atom in **3** is shortened to 2.0283(5) Å from 2.0918(7) Å in **2**. To the best of our knowledge, the shortest structurally characterized Mn-P bond prior to this publication was reported by Gudat et al. in a monodentate NHP manganese carbonyl complex $(^{Dipp}NHP)Mn(CO)_4$ (Dipp = 2,6-diisopropylphenyl) at 2.063(1) Å,[30] making the Mn-P bond in **3** the shortest Mn-P bond distance to date. The geometry of the central P^{NHP} atom is essentially planar, with the sum of its angles equaling 358°. In addition, **3** features an angle of 170.3° between the N-P-N plane and the P^{NHP}-Mn bond vector (NHP bend angle), which differs from those of complexes featuring pyramidal NHP phosphorus atom geometries described as NHP^- phosphido complexes due to a stereochemically active lone pair (120°-130°),[43,44] and is more comparable to the NHP bend angles in NHP^+ phosphenium complexes containing planar P^{NHP} geometries (~160°).[43] For comparison, the NHP bend angle in complex **2**, which contains a trigonal pyramidal geometry about the NHP phosphorus atom since it is bound to a halide, was measured at 138.3°. These bond metrics further highlight the planarity of the P^{NHP} atom in **3**.

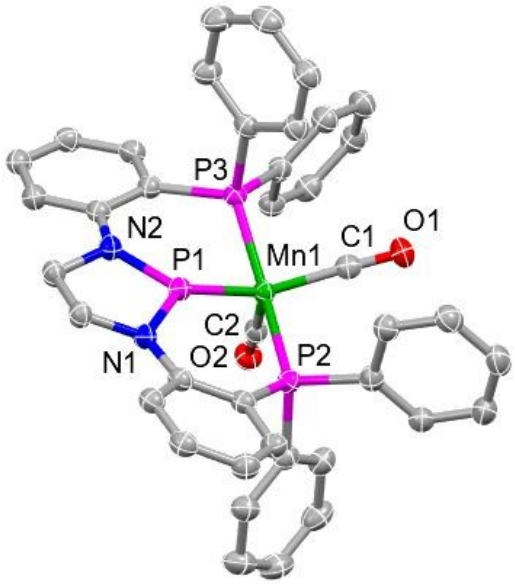

Figure 4. Displacement ellipsoid (50%) representation of **3**. All hydrogen atoms have been omitted for clarity. Relevant bond distances (Å) and angles (°): Mn1-P1, 2.0283(5); Mn1-P2, 2.2362(5); Mn1-P3, 2.2206(5); Mn1-C1, 1.8106(18); Mn1-C2, 1.7713(18); C1-O1, 1.154(2); C2-O2, 1.166(2); P1-Mn1-C1, 145.35(5); P1-Mn1-C2, 112.95(6); P2-Mn1-P3, 169.07(2).

We hypothesized that Mn-P multiple bonding character could account for both the short Mn-P distance and the planarity about the P^{NHP} atom; thus, computational studies were performed

using DFT and natural bond orbital (NBO) analysis to provide further insight into the Mn-P^{NHP} bonding interaction. Geometry optimizations were carried out starting from the crystallographically derived Cartesian coordinates of **3** and resulted in similar bond metrics to the experimental values (Table S12). Two bonding interactions between the Mn center and P^{NHP} atom were modeled in an NBO analysis of **3** (Figure 5). One of the Mn-P NBOs was found to be strongly polarized toward phosphorus (67.3% P / 32.7% Mn), indicative of dative donation of the phosphorus lone pair to the Mn center (Table S13). In addition, the Mn-P interaction is further strengthened by a π-interaction that was found to be more covalent in nature with similar constitution (41.2% Mn / 58.8% P). The phosphorus orbital involved in this π-bond was constituted almost entirely of p orbital character (95.4%). A Mn-P double bond is consistent with the short Mn-P^{NHP} distance and planarity about the phosphorus atom observed in **3**. However, given the covalency of the Mn-P π-interaction, the polarity of the Mn-P^{NHP} bond remains unclear in that **3** could be described as (1) a Mn^{-I} with Mn→P π-backbonding to a phosphenium (NHP^{+}) ligand or (2) a Mn^{I} complex with P→Mn π-donation from a phosphido (NHP^{-}) ligand (*vide infra*).

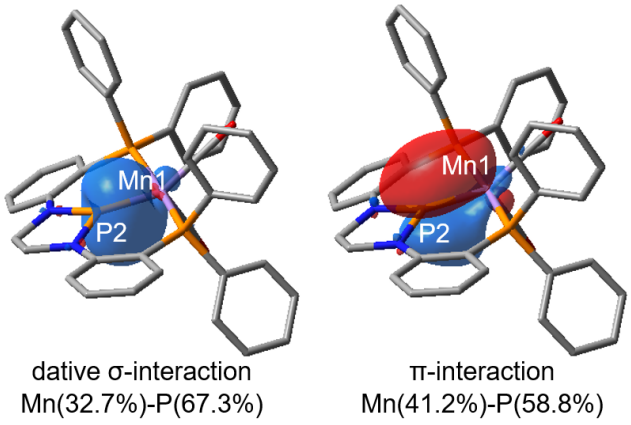

Figure 5. Pictorial representations of the calculated σ- and π-bonding interactions (NBO analysis) in **3**.

The Mn center adopts a distorted square pyramidal geometry with a τ_5 value[45] of 0.40. However, a square pyramidal geometry is in stark contrast to the solution-phase ^{1}H NMR data, which suggests a more symmetric trigonal bipyramidal Mn center since the protons on the carbon backbone of the heterocycle are equivalent on the NMR timescale. Thus, we turned to IR spectroscopy to probe whether the crystallographically determined solid-state structure of **3** was representative of the structure in solution. By solid-state IR spectroscopy, two carbonyl stretching modes were observed at 1906 and 1836 cm^{-1} (Figure S17). Although these stretching frequencies are comparable to the range of those in dicarbonyl Mn^{I} complexes (2000-1800 cm^{-1}),[9,20,22,27,42,46–53] the electronic description of the Mn center and P^{NHP} atom remains ambiguous as the electron-withdrawing effects of a cationic NHP^{+} ligand toward a Mn^{-I} center may yet account for the observation of higher stretching frequencies. In solution, both of the stretches observed in the solid-state IR spectrum are present at 1906 and 1837 cm^{-1}, but a second set of stretches is observed at 1912 and 1850 cm^{-1} (Figure S18). Thus, we posit that a fluxional process that interconverts square pyramidal and trigonal bipyramidal geometries about the Mn center occurs in solution and is too fast to detect on the slower timescale of NMR experiments but slow enough to capture by IR spectroscopy. Indeed, computational studies revealed that the square pyramidal and trigonal bipyramidal isomers were similar in energy (within 0.5 kcal/mol, see Tables S14-S16). Variable temperature NMR spectra of **3** were collected, but no changes in peak shape were observed by either $^{31}P\{^1H\}$ or ^{1}H NMR spectroscopy from room temp down to -80 °C (Figures S15-S16). Thus, while **3** rapidly interconverts between square pyramidal and trigonal bipyramidal geometries in solution, the square pyramidal geometry is dominant in the solid state.

Reactivity of (PPP)Mn(CO)$_2$ with Ammonia Borane. Building upon our initial inspiration from Mn hydrogenation catalysts, we sought to apply complex **3** as a hydrogenation catalyst toward unsaturated substrates. Unfortunately, the addition of H_2 gas (1-70 bar) to **3** at various temperatures (27-130 °C) for 24-72 hours resulted in no spectroscopic changes, with only minimal decomposition observed under even the harshest conditions (Figure S19). Acetophenone was added to **3**, pressurized with H_2 gas, and heated in an attempt to drive hydrogenation should an H_2-activated complex be generated *in situ*; however, only unreacted starting materials were observed by ^{1}H and $^{31}P\{^1H\}$ NMR spectroscopy (Figures S20-S21). We hypothesized that a more stepwise addition of substrates rather than the addition of nonpolar H_2 would allow for more facile bond activations owing to the polarity of the Mn-P^{NHP} bond in **3**.

Scheme 3. Formation of (PP^HP)Mn(CO)$_2$H Using NH_3BH_3

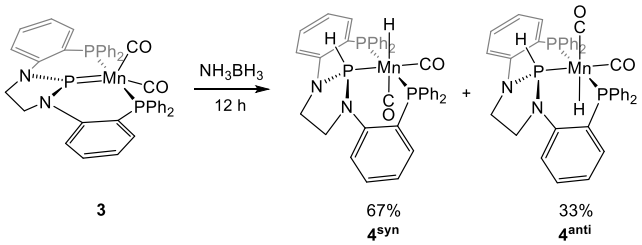

As such, we studied complex **3**'s reactivity with ammonia borane, a polarized source of H_2 that is well-studied and implemented in metal-catalyzed hydrogenations.[54] The catalytic dehydrogenation of ammonia borane using (^{Dipp}NHP)Mn(CO)$_4$ was demonstrated by Gudat et al. although an H_2-addition species (^{Dipp}NHP-H)Mn(CO)$_4$H was only isolable through treatment of (^{Dipp}NHP)Mn(CO)$_4$ with a hydride source and subsequent protonation with [HNEt$_3$]Cl.[30] The addition of one equivalent of NH_3BH_3 to **3** affords a mixture of isomers of (PP^HP)Mn(CO)$_2$H (**4**), the product of formal addition of H_2 across the Mn-P bond, after 12 hours (Scheme 3). Although dehydrogenated byproducts of NH_3BH_3 were not detected by NMR spectroscopy, an insoluble white precipitate was observed over the course of several hours, and these solids are likely attributed to insoluble NH_3BH_3 dehydrogenation products such as polyaminoboranes. The $^{31}P\{^1H\}$ NMR spectrum of **4** contains two products with very similar chemical shifts, each with corresponding P^{NHP} atom and PPh_2 sidearm resonances integrating in a 1:2 ratio, respectively. The $^{31}P\{^1H\}$ NMR resonances of the major product in mixture **4** are a triplet at 156.0 ppm and doublet at 72.9 ppm, and the P^{NHP} and PPh_2 sidearm resonances of the minor product are nearly identical to those of the major product, corresponding to 157.8 ppm and 72.2 ppm, respectively. Variable temperature ^{1}H and $^{31}P\{^1H\}$ NMR spectra of the 2:1 mixture of species in **4** show no spectroscopic change in the ratio at elevated temperatures (Figures S28-S29), suggesting that the two products do not interconvert via an

equilibrium process. In addition, while the use of excess NH_3BH_3 (10 equivalents) was shown to greatly accelerate the formation of **4** by reaching completion in just 1 hour, the ratio of major and minor products remained unchanged (Figure S35).

Similar to the potential for stereoisomerism described for precursor **2**, we postulated that the two isomers of **4** observed spectroscopically differ by the orientation of the Mn-H bond. To aid in assignment of the major and minor products of **4**, computational studies were performed. The three stereoisomers of **4** where the Mn-H bond is oriented trans to the P^{NHP} atom ($\mathbf{4}^{\mathbf{trans}}$), cis to the P^{NHP} atom and syn to the P^{NHP}-H bond ($\mathbf{4}^{\mathbf{syn}}$), or cis to the P^{NHP} atom and anti to the P^{NHP}-H bond ($\mathbf{4}^{\mathbf{anti}}$) were optimized to a minimum using DFT (Tables S17-S19). Frequency calculations (Table S20) were subsequently performed and revealed that the $\mathbf{4}^{\mathbf{syn}}$ stereoisomer was the lowest in energy by -6.9 kcal/mol, followed by the $\mathbf{4}^{\mathbf{anti}}$ stereoisomer at -6.7 kcal/mol relative to $\mathbf{4}^{\mathbf{trans}}$ (Figure 6). Based on these results, $\mathbf{4}^{\mathbf{trans}}$ is likely not one of the observed isomers. The small difference (0.2 kcal/mol) in calculated free energies of $\mathbf{4}^{\mathbf{syn}}$ and $\mathbf{4}^{\mathbf{anti}}$ is consistent with the observation of both isomers but does not provide sufficiently strong evidence as to which isomer corresponds to the major or minor product of **4**, specifically. A similar mixture of isomers was also noted in a study of a CNP-supported dicarbonyl Mn species $(CN^HP)Mn(CO)_2H$ by Filonenko, Pidko, and coworkers, who also spectroscopically observed a mixture of isomers by the respective positions of the axial carbonyl and hydride ligands relative to the meridionally-bound CN^HP ligand.[49] Nonetheless, $\mathbf{4}^{\mathbf{syn}}$ and $\mathbf{4}^{\mathbf{anti}}$ likely comprise the two species in mixture **4**.

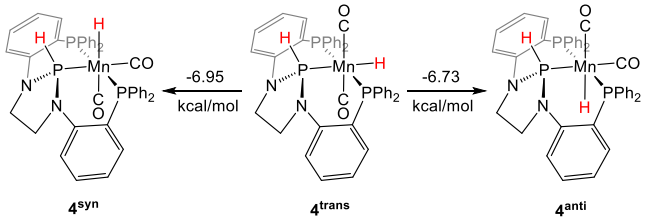

Figure 6. Free energy calculations of $\mathbf{4}^{\mathbf{syn}}$, $\mathbf{4}^{\mathbf{trans}}$, and $\mathbf{4}^{\mathbf{anti}}$.

The successful formation of the Mn-H and P^{NHP}-H bonds in both $\mathbf{4}^{\mathbf{syn}}$ and $\mathbf{4}^{\mathbf{anti}}$ was discerned by ^{31}P and ^1H NMR spectroscopy. Two nearly overlapping resonances in a 1:2 integral ratio were observed in the metal hydride region of the ^1H NMR spectrum: a doublet of triplets at -7.65 ppm (minor product) and a doublet of doublet of triplets at -7.81 ppm (major product) (Figure S22). Each metal hydride integrates to one proton with respect to each isomer's corresponding NHP backbone resonances. Interestingly, coupling between the metal hydride and P^{NHP}-H proton ($^3J_{H\text{-}H}$ = 14 Hz) is only observed in the major product of **4**. Guan and coworkers recently reported pincer-ligated iron carbonyl complexes $(^{iPr}PP^HP)FeH(CO)Cl$ in which the P-H bond installed in the central position of the tridentate ligand and the metal hydride bond may adopt either a syn or anti configuration to one another. Notably, weak coupling ($^3J_{H\text{-}H}$ = 8.4 Hz) between the P-bound proton and the metal hydride was only reported in *syn*-$(^{iPr}PP^HP)FeH(CO)Cl$, with no three-bond H-H coupling observed in the ^1H NMR spectrum of *anti*-$(^{iPr}P\text{-}P^HP)FeH(CO)Cl$.[55] Based on this similar coupling information, the major product of **4** was assigned as $\mathbf{4}^{\mathbf{syn}}$ and the minor product as $\mathbf{4}^{\mathbf{anti}}$. Additional strong coupling ($^1J_{P\text{-}H}$ = 375 ($\mathbf{4}^{\mathbf{syn}}$), 329 ($\mathbf{4}^{\mathbf{anti}}$) Hz) observed in the P^{NHP} atom resonances of the ^{31}P NMR spectrum of **4** was indicative of the formation of the P^{NHP}-H bond (Figures S25-S26) and comparable to other reported NHP first-row transition metal complexes (300-400 Hz).[30,33,34,38] By ^1H NMR spectroscopy, the P^{NHP}-H resonances were found to overlap with multiple signals in the aromatic region. To definitively assign these resonances, ^{31}P-decoupling was used to decouple proton resonances from the central P^{NHP} atom, resulting in collapse to a doublet centered at 7.48 ppm with a $^3J_{H\text{-}H}$ coupling constant of 14 Hz and a singlet at 7.28 ppm, corresponding to $\mathbf{4}^{\mathbf{syn}}$ and $\mathbf{4}^{\mathbf{anti}}$, respectively (Figure 7). To further support this assignment, a deuterated analogue of **4** was synthesized using ND_3BD_3 in an analogous procedure to afford $(PP^DP)Mn(CO)_2D$ ($\mathbf{4}$-$\boldsymbol{d_2}$). The ^1H and $^{31}P\{^1H\}$ NMR spectroscopic data of $\mathbf{4}$-$\boldsymbol{d_2}$ matched those of **4**, with the exception of the absence of P^{NHP}-H and Mn-H resonances to further confirm that the source of H_2 transfer to **3** was indeed ammonia borane. ^2H NMR spectroscopy of $\mathbf{4}^{\mathbf{anti}}$-$\boldsymbol{d_2}$ and $\mathbf{4}^{\mathbf{syn}}$-$\boldsymbol{d_2}$ allowed for definitive assignment of the P^{NHP}-H/D chemical shifts and coupling constants of $\mathbf{4}^{\mathbf{anti}}$ and $\mathbf{4}^{\mathbf{syn}}$ in the absence of overlapping aromatic resonances (Figure 7). The P^{NHP}-D resonances for $\mathbf{4}^{\mathbf{anti}}$-$\boldsymbol{d_2}$ and $\mathbf{4}^{\mathbf{syn}}$-$\boldsymbol{d_2}$ were clearly observed centered at 7.28 ppm and 7.48 ppm, respectively, in the ^2H NMR spectrum, and the observed coupling constants were in excellent agreement with those observed by ^{31}P NMR spectroscopy (Figures S36-S39). Furthermore, the ^1H-^1H COSY NMR spectrum of **4** was used to correlate the metal hydride resonances with each isomer's corresponding P^{NHP}-H resonance (Figure S32), providing confident spectroscopic assignments of the Mn-H and P^{NHP}-H protons of $\mathbf{4}^{\mathbf{syn}}$ and $\mathbf{4}^{\mathbf{anti}}$.

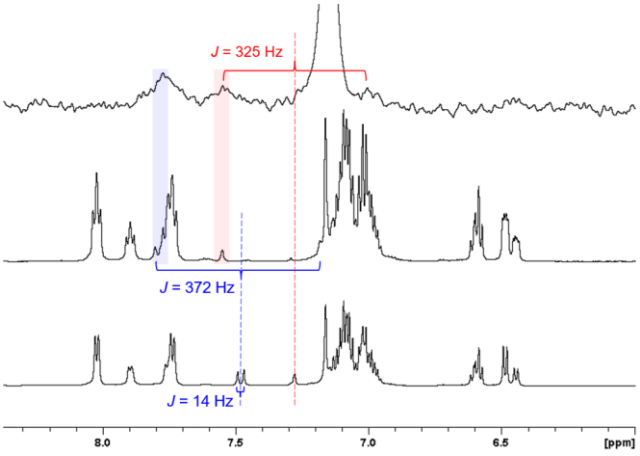

Figure 7. Aromatic region of the (top) ^2H NMR spectrum (92.1 MHz, C_6H_6) of $\mathbf{4}$-$\boldsymbol{d_2}$, (middle) ^1H NMR spectrum (600 MHz, C_6D_6) of **4**, and (bottom) $^1H\{^{31}P\}$ NMR spectrum (600 MHz, C_6D_6) of **4**. The P^{NHP}-H resonance of $\mathbf{4}^{\mathbf{syn}}$ (7.48 ppm) is shown in blue, and its coupling to the central P^{NHP} atom ($^1J_{H\text{-}P}$ = 372 Hz) is shown by ^1H NMR (middle) and coupling to the metal hydride ($^3J_{H\text{-}H}$ = 14 Hz) is more clearly shown by $^1H\{^{31}P\}$ NMR (bottom). The P^{NHP}-H resonance of $\mathbf{4}^{\mathbf{anti}}$ (7.28 ppm) is shown in red, and its coupling to the central P^{NHP} atom is best shown in the ^2H NMR spectrum of $\mathbf{4}^{\mathbf{anti}}$-$\boldsymbol{d_2}$ ($^1J_{D\text{-}P}$ = 325 Hz) (top). To further support the presence of P^{NHP}-H/D resonances overlapping with that of residual solvent, spectroscopic data were also collected in THF/THF-d_8 and resonances identified (Figures S31 and S39).

The mixture of $\mathbf{4}^{\mathbf{syn}}/\mathbf{4}^{\mathbf{anti}}$ was also characterized using IR spectroscopy. The P^{NHP}-H stretches for the two isomers could not be distinguished as a single broad feature was observed at 2205 cm^{-1}, which is similar to those of other transition metal P^{NHP}-H

complexes.[30,34,38,56] In addition, two CO stretching frequencies were observed at 1938 and 1871 cm^{-1} for **4** (Figure S34). The frequencies calculated using DFT calculations for $\mathbf{4}^{anti}$ and $\mathbf{4}^{syn}$ are relatively similar (within ~15 cm^{-1}) and in good agreement with the experimental values (Figures S44-S46). We posit that the CO stretches of $\mathbf{4}^{anti}$ and $\mathbf{4}^{syn}$ are too similar in energy to be distinguished in the 2:1 mixture of products. The observed similar intensities of the symmetric and asymmetric CO stretches are inconsistent with $\mathbf{4}^{trans}$, which should have a much smaller symmetric stretch, further allowing us to rule out this possibility.

Stepwise Proton/Hydride Addition to (PPP)Mn(CO)$_2$. Ultimately, the polarized E-H (E = B, N) bonds of NH_3BH_3 were required to add one equivalent of H_2 to complex **3** to form **4**, as the addition of H_2 gas resulted in no observable change. To investigate the nature of the P^{NHP}-Mn bond and probe the nucleophilicity or electrophilicity of the Mn and P centers, reactivity studies using acid, base, and hydride sources for $H^{+/-}$ transfer were performed.

Scheme 4. Synthesis of $(PP^{Cl}P)Mn(CO)_2H$ and $K(THF)_2[(PP^{H}P)Mn(CO)_2]$ via addition of H^+ and H^- to 3.

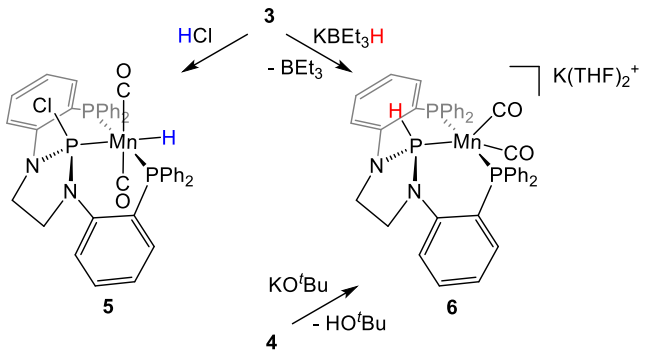

The addition of HCl to **3** generates the metal hydride species $(PP^{Cl}P)Mn(CO)_2H$ (**5**) with an immediate color change from orange to bright yellow (Scheme 4). The P^{NHP} resonance in the $^{31}P\{^1H\}$ NMR spectrum of **5** appears at 182.9 ppm, which is similar to the P^{NHP} resonance of the chlorophosphine in **2** (181.4 ppm). A doublet of triplets is observed in the metal hydride region of the ^1H NMR spectrum at -8.06 ppm, with coupling to the central P^{NHP} atom ($^2J_{H\text{-}P}$ = 50 Hz) and the phosphine sidearms ($^2J_{P\text{-}PPh2}$ = 91 Hz) (Figure 8). This coupling ($^2J_{P\text{-}H}$ = 50 Hz) is also observed by ^{31}P NMR spectroscopy in the NHP phosphorus atom resonance and is significantly smaller than reported values of P^{NHP}-H bonds and that of **4**,[33,34,36,37,56–58] further supporting the installation of a metal hydride upon protonation of a nucleophilic Mn center and chloride binding to an electrophilic phosphenium ligand in **3**.

By IR spectroscopy, two CO stretching frequencies were observed for **5** at 1947 and 1891 cm^{-1} (Figure S52). These values are lower than those observed in **2** (νCO: 1971, 1933 cm^{-1}), likely due to the installation of the metal hydride in place of the more electron-withdrawing halide ligand on the Mn center in **2**. Similarly, the CO stretches in **5** were higher than those of **4** (νCO: 1938, 1871 cm^{-1}) likely owing to the P^{NHP}-H bond in **4** in comparison to the P^{NHP}-Cl moiety in **5**. Altogether, these results are consistent with a decreasing trend in CO stretching frequencies with less electron-withdrawing substituents in complexes **2**, **4**, and **5**. The formation of **5** upon protonation indicates that the P^{NHP} atom is not the most basic site in complex **3**.

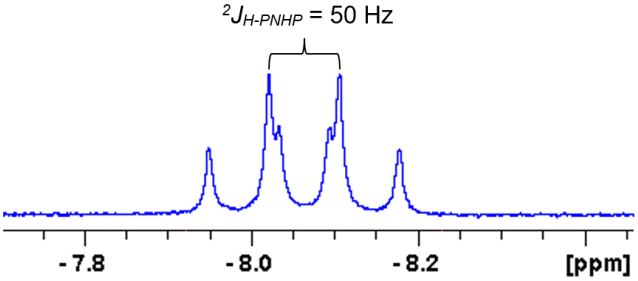

Figure 8. Metal hydride resonance in the ^1H NMR spectrum of **5** (600 MHz, C_6D_6). Two-bond coupling to the central NHP phosphorus atom is observed ($^2J_{H\text{-}PNHP}$ = 50 Hz).

Conversely, the addition of $KBEt_3H$ to complex **3** afforded an anionic complex $K(THF)_2[(PP^{H}P)Mn(CO)_2]$ (**6**) featuring a P^{NHP}-H bond (Scheme 4). Owing to **6**'s proclivity for thermal decomposition in solution, full characterization data could not be obtained. However, the significantly poorer solubility of **6** in comparison to **5** can be accredited to its composition as a potassium salt. To further support this anionic Mn^{-I} species, two CO stretches were identified by IR spectroscopy at 1762 and 1701 cm^{-1} (Figure S58), which are markedly lower than the 2000-1800 cm^{-1} range observed in complexes **2**, **4**, and **5** and other Mn^{I} carbonyl species.[22,23,40,42,46,48,49] Tondreau and coworkers report the decrease of CO stretching frequencies as a result of decreasing overall charge in a PNP-supported cationic Mn^{I} dicarbonyl complex [(^{tBu}PNNOP)Mn(CO)$_2$][Br] (^{tBu}PNNOP = 2,6-(di-*tert*-butylphosphinito)(di-*tert*-butylphosphinamine)pyridine) (νCO = 1939, 1869 cm-^{1}) upon dehydrohalogenation to afford the neutral Mn^{I} species (^{tBu}PNNOP)Mn(CO)$_2$ (νCO = 1914, 1842 cm^{-1}).[48] In addition to the effects of overall charge, Tonzetich and coworkers observe markedly lower CO stretching frequencies upon decreasing metal oxidation state in 5-coordinate pyrrole-based PNP complexes [(^{tBu}dPNP-H)$Mn^{I}(CO)_2]^+$ (νCO = 1942, 1871 cm^{-1}), (^{tBu}PNP)$Mn^{I}(CO)_2$ (νCO = 1904, 1833 cm^{-1}), and [(^{tBu}PNP)$Mn^{0}(CO)_2]^-$ (νCO = 1817, 1722 cm^{-1}).[59] The trends observed in the CO stretching frequencies of these previously reported series are consistent with our observation of higher stretching frequencies for neutral Mn^{I} complexes **2**, **4**, and **5** and lower stretching frequencies for anionic Mn^{-I} complex **6**. Thus, we attribute the lower CO stretching frequencies in the IR spectrum of **6** to both the overall negative charge of the metal-containing portion as well as the change in oxidation state to a Mn^{-I} center.

The formation of the P^{NHP}-H bond in **6** was confirmed by NMR spectroscopy. In the $^{31}P\{^1H\}$ NMR spectrum, the central NHP phosphorus atom resonance was located at 142.2 ppm as a triplet. Additional strong coupling ($^1J_{P\text{-}H}$ = 362 Hz) to the P^{NHP}-H atom was observed in the P^{NHP} resonance without ^1H-decoupling, and is of similar large magnitude to the P^{NHP}-H coupling in $\mathbf{4}^{syn}$ ($^1J_{P\text{-}H}$ = 375 Hz), $\mathbf{4}^{anti}$ ($^1J_{P\text{-}H}$ = 329 Hz), and other P^{NHP}-H complexes.[33,34,36,37,56–58] A broad doublet in the P^{NHP}-H region of the ^1H NMR spectrum centered at 7.70 ppm featured this same coupling constant ($^1J_{H\text{-}P}$ = 362 Hz) while no signals were found in the metal hydride region (Figure 9). In addition, this P^{NHP}-H resonance collapses to a broad singlet at 7.70 ppm when decoupled to the central NHP phosphorus atom by $^1H\{^{31}P\}$ NMR spectroscopy (Figure 9), further supporting the installation of a P^{NHP}-H bond upon the reaction of **3** with $KBEt_3H$ as a source of H^-. The generation of **6** via hydride addition indicates that the P^{NHP} atom is electrophilic.

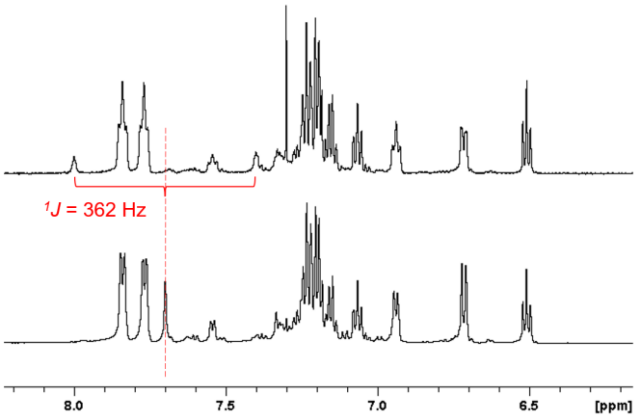

Figure 9. Aromatic region of the (top) ^{1}H NMR spectrum and (bottom) ^{1}H{^{31}P} NMR spectrum of **6** (600 MHz, THF-d_8). The ^{1}H{^{31}P} NMR spectrum is decoupled to the central NHP phosphorus atom resonance (142.3 ppm) in the ^{31}P NMR spectrum of **6**. The P^{NHP}-H resonance of **6** is centered at 7.70 ppm, and its large coupling to the central NHP phosphorus atom is shown in the ^{1}H NMR spectrum as a broad doublet ($^{1}J_{H\text{-}PNHP}$ = 362 Hz).

In light of the limited characterization of **6**, we turned to alternate synthetic pathways to support the formation of **6** via exploitation of the nucleophilic Mn center and electrophilic phosphenium moiety within this manganese system. Since a hydride could be used to install the P^{NHP}-H bond to **3** while protonation of **3** occurred at the Mn center, we posited that that the addition of base to **4** would also generate **6** via deprotonation of the acidic Mn-H bond. The addition of one equivalent of KO^{t}Bu to **4** resulted in an immediate color change from pale, light-yellow to a dark orange-red color and greatly reduced solubility, both of which are characteristic of **6**. Indeed, the formation of complex **6** was confirmed by ^{31}P{^{1}H} NMR spectroscopy (Figure S61), indicating deprotonation of the Mn-hydride while the P^{NHP}-H bond was preserved. Likewise, the P^{NHP}-H moiety in **6** could not be deprotonated with KO^{t}Bu due to its hydridic nature (Figure S62). The nucleophilic nature of the Mn center and electrophilic behavior of the P^{NHP} atom in this (PPP)Mn system substantiated by these reactivity studies suggest significant contribution from the NHP^{+}/Mn^{-I} resonance form of **3** rather than an NHP^{-}/Mn^{I} complex description.

CONCLUSION

In conclusion, the initial coordination of the [PPP]Cl ligand scaffold to a manganese center was achieved using $Mn(CO)_5Br$ and irradiation with 254 nm light to afford $(PP^{Cl}P)Mn(CO)_2Br$ (**2**). Careful control of reagent scale and solvent volume was required to minimize halide exchange and the formation of stereoisomers of **2**. However, mixtures of $(PP^{X}P)Mn(CO)_2X$ isomers converged to a single product upon reduction with two equivalents of KC_8, generating a coordinatively-unsaturated pincer-ligated dicarbonyl manganese species, $(PPP)Mn(CO)_2$ (**3**). The identification of both σ- and π-bonding interactions between the Mn center and the planar P^{NHP} atom was consistent with the very short P^{NHP}-Mn bond in **3**. However, the direction of polarity of the Mn-P^{NHP} bond based on physical parameters alone remained ambiguous since the additional π-interaction could be described as either the donation of a lone pair from an NHP^{-} ligand to a Mn^{I} center or backbonding from a Mn^{-I} center to an NHP^{+} ligand. While no reaction between H_2 and **3** was observed, the generation of $(PP^{H}P)Mn(CO)_2H$ (**4**) was achieved upon reaction of **3** with NH_3BH_3. The metal-bound hydrogen atom can be removed as H^{-} using the base KO^{t}Bu to afford the salt $K(THF)_2[(PP^{H}P)Mn(CO)_2]$ (**6**), which can also be accessed by reaction of $KBEt_3H$ with **3**, highlighting the more hydridic nature of the phosphorus-bound hydrogen atom. Accordingly, the nucleophilicity of the Mn center was demonstrated through selective protonation at Mn rather than phosphorus upon addition of HCl to **3**, resulting in the formation of metal hydride species $(PP^{Cl}P)Mn(CO)_2H$ (**5**). These reactivity studies revealed the electrophilic nature of the N-heterocyclic phosphenium moiety that gives rise to the inverse metal-ligand electronics of $(PPP)Mn(CO)_2$ as a NHP^{+}/Mn^{-I} complex, in comparison to previously reported pincer-ligated dicarbonyl Mn^{I} species (Figure 1) and to $(PPP)Co(PMe_3)$ NHP^{-}/Co^{I} complex (Chart 2). Future studies will leverage the complex interactions between the Earth-abundant Mn center and the N-heterocyclic phosphenium moiety in these (PPP) pincer systems toward applications in small molecule activation and catalysis.

EXPERIMENTAL SECTION

General Considerations. All manipulations were carried out under an inert atmosphere using a nitrogen-filled glovebox or standard Schlenk techniques. Glassware was oven-dried before use. All solvents were degassed by sparging with ultra-high purity argon and dried via passage through columns of drying agents using a Seca solvent purification system from Pure Process Technologies. C_6D_6, CD_2Cl_2, and THF-d_8 were purchased from Cambridge Isotopes Laboratories, dried over CaH_2, distilled, degassed by repeated freeze-pump-thaw cycles, and stored over pre-activated 3 Å molecular sieves. [PPP]Cl (**1**) and [PPP]Br were synthesized according to literatures procedures.[32,60] Potassium (98% in mineral oil) was purchased from Acros Organics and washed with hexanes. Graphite powder (99.9%, -20+100 mesh) was purchased from Alfa Aesar and dried under vacuum at 200-300 °C for 3 days. KC_8 was prepared by mixing 1.1 equivalents of potassium with 1 equivalent of graphite powder in a vial and heating to 100 °C while occasionally shaking the vial until the silver-colored potassium melted and changed to a mustard gold color (approximately 5-10 min). Isopropanol was purchased from Fisher Chemical, distilled, and stored over 3 Å molecular sieves. KO^{t}Bu (98+%) was purchased from Acros Organics and further dried under vacuum at 120 °C overnight prior to use. Acetophenone (99%) was purchased from Alfa Aesar, distilled, and stored over 3 Å molecular sieves. NH_3BH_3 (97%) was purchased from Sigma Aldrich, sublimed, and dried under vacuum for 24 h. $NaBD_4$ (D4, 99%; 95% chemical purity) and $(ND_4)_2SO_4$ (D8, 98%) were purchased from Cambridge Isotope Laboratories, and ND_3BD_3 was synthesized using an analogous literature procedure for NH_3BH_3,[61] sublimed, and dried under vacuum for 24 h. All other chemicals were purchased from commercial vendors and used without further purification. A RMR-600 Rayonet Mini-Photochemical chamber reactor equipped with RMR-2537A lamps (254 nm bulbs) and a fan was used to irradiate reaction vessels. NMR data were recorded at ambient temperature unless otherwise stated on a Bruker DPX 400 MHz instrument, Bruker AVANCE III HD 600 MHz instrument, or Bruker AVANCE III HD Ascend 700 MHz instrument equipped with 5 mm triple-resonance observe (TXO) cryoprobe and Z-axis gradients. Chemical shifts are reported in δ units in ppm referenced to residual solvent peaks (^{1}H and ^{13}C{^{1}H} NMR).[62] ^{31}P{^{1}H} and ^{31}P NMR chemical shifts are referenced using an 85% H_3PO_4 external standard (0 ppm). ^{11}B{^{1}H} NMR chemical shifts are referenced using a BF_3•Et_2O external standard (0 ppm). Solution infrared spectra were recorded on a Bruker TENSOR II spectrometer controlled by OPUS software. Solid-state attenuated total reflection (ATR) infrared spectra were recorded on a Bruker ALPHA II spectrometer controlled by OPUS software. Microanalysis data (CHN) were collected by Midwest Microlab, Indianapolis, IN.

$(PP^{Cl}P)Mn(CO)_2Br$ (2). $Mn(CO)_5Br$ (17 mg, 0.061 mmol) and [PPP]Cl (**1**) (39 mg, 0.061 mmol) were added to a 100 mL Schlenk tube and dissolved in THF (30 mL). The headspace of the reaction vessel

was removed *in vacuo* (2-3 min). The Schlenk tube was then sealed under vacuum and irradiated with 254 nm light for 12 h. Upon reaction, the yellow solution turned an orange color. The solvent was then removed from the reaction mixture *in vacuo*. The resulting orange solid was extracted with CH_2Cl_2 (10 mL) and filtered through glass microfiber filter paper. The solvent from the filtrate was removed *in vacuo* yielding **2** as an orange solid (48 mg, 94%). Crystals of **2** suitable for X-ray diffraction were grown via layering a concentrated CH_2Cl_2 solution of **2** with *n*-pentane. ^{1}H NMR (600 MHz, CD_2Cl_2): δ 7.61 (m, Ar-H, 4H), 7.54 (m overlapping signals, Ar-H, 6H), 7.46-7.40 (m overlapping signals, Ar-H, 6H), 7.40-7.31 (m overlapping signals, Ar-H, 6H), 7.10 (m, Ar-H, 2H), 6.95 (m, Ar-H, 2H), 6.88 (m, Ar-H, 2H), 4.07 (br s, CH_2CH_2, 2H), 3.77 (br s, CH_2CH_2, 2H). ^{31}P{^{1}H} NMR (242.9 MHz, CD_2Cl_2): δ 181.4 (br t, P^{NHP}, $^2J_{P\text{-}PPh2}$ = 75 Hz, 1P), 51.9 (d, PPh_2, $^2J_{P\text{-}PNHP}$ = 76 Hz, 2P). ^{13}C{^{1}H} NMR (159.0 MHz, CD_2Cl_2): δ 217.8 (m, CO), 146.7 (m, *ipso*), 136.8 (m, *ipso*), 136.7 (s), 134.5 (m, *ipso*), 134.2 (s), 133.1 (s), 132.8 (s), 130.0 (s), 129.7 (s), 128.0 (s), 127.9 (s), 122.3 (s), 118.8 (m, *ipso*), 117.6 (s), 46.2 (s, CH_2CH_2). IR (CH_2Cl_2): 1971 cm^{-1}, 1933 cm^{-1}. Anal. Calcd for $C_{40}H_{32}MnN_2O_2P_3ClBr$: C, 57.47; H, 3.86; N, 3.35. Found: C, 56.84; H, 4.09; N, 3.23.

Generation of ($PP^{Br}P$)Mn(CO)$_2$Br. ($PP^{Br}P$)Mn(CO)$_2$Br was synthesized via an analogous procedure to **2** using [PPP]Br (**1-Br**). $Mn(CO)_5Br$ (29 mg, 0.073 mmol) and **1-Br** (49 mg, 0.071 mmol) were added to a 100 mL Schlenk tube and dissolved in THF (30 mL). The headspace of the reaction vessel was removed *in vacuo* (2-3 min). The Schlenk tube was then sealed under vacuum and irradiated with 254 nm light for 16 h. Upon reaction, the yellow solution turned an orange color. The solvent was then removed from the reaction mixture *in vacuo*, leaving 58 mg of a crude orange solid. Without purification, the ^{31}P{^{1}H} NMR chemical shifts were compared to those generated in various synthetic attempts to generate **2** under different conditions. ^{31}P{^{1}H} NMR (162.0 MHz, THF): δ 174.2 (br t, P^{NHP}, $^2J_{P\text{-}PPh2}$ = 73 Hz, 1P), 52.9 (d, PPh_2, $^2J_{P\text{-}PNHP}$ = 73 Hz, 2P).

(PPP)Mn(CO)$_2$ (3). Complex **2** (306 mg, 0.366 mmol) was dissolved in THF (10 mL) and added to a stirring suspension of KC_8 (98.9 mg, 0.732 mmol) in THF (8 mL). The solution darkened gradually and was stirred at room temperature for 2 h. The reaction mixture was then filtered through Celite to remove the black graphite solids. The solvent was removed from the dark orange filtrate *in vacuo*, and the resulting dark orange solid was then washed with C_6H_6 (15 mL) and collected on a pad of Celite on a sintered glass frit. THF (2 mL) was then used to wash the collected solids three times, allowing the THF to stand the Celite pad for ~3 min each time before vacuum filtration. A dark brown impurity that was found to be more soluble in THF than desired product **3** was removed via this method. The ~3 min waiting period was found to be imperative for removing the dark impurities while minimizing loss of product **3** (i.e. pushing THF through the filter immediately after addition does not sufficiently separate the mixture and instead results in significant loss of desired product **3**). After washing with THF, the bright orange solid remaining on the Celite pad was extracted with CH_2Cl_2 (16 mL) and filtered through the Celite. The solvent was removed from the filtrate *in vacuo*, yielding **3** as a bright orange solid (118 mg, 45%). Crystals of **3** suitable for X-ray diffraction were grown via layering a concentrated CH_2Cl_2 solution of **3** with *n*-pentane. ^{1}H NMR (600 MHz, CD_2Cl_2): δ 7.66 (m, Ar-H, 2H), 7.56-7.52 (m overlapping signals, Ar-H, 8H), 7.35-7.29 (m overlapping signals, Ar-H, 12H), 7.11 (m, Ar-H, 2H), 7.05-7.03 (m, Ar-H, 2H), 3.94 (br s, CH_2CH_2, 4H). ^{31}P{^{1}H} NMR (242.9 MHz, CD_2Cl_2): δ 203.8 (t, P^{NHP}, $^2J_{P\text{-}PPh2}$ = 159 Hz, 1P), 67.0 (d, PPh_2, $^2J_{P\text{-}PNHP}$ = 157 Hz, 2P). ^{13}C{^{1}H} NMR (150.9 MHz, CD_2Cl_2): δ 229.6 (m, CO), 146.7 (m, *ipso*), 140.2 (m, *ipso*), 133.5 (s), 133.0 (s), 130.7 (s), 129.2 (s), 128.1 (s), 121.9 (s), 117.9 (m, *ipso*), 115.6 (s), 47.2 (s, CH_2CH_2). IR (CH_2Cl_2): 1912 cm^{-1}, 1906 cm^{-1}, 1850 cm^{-1}, 1837 cm^{-1}. IR (ATR): 1906 cm^{-1}, 1836 cm^{-1}. Anal. Calcd for $C_{40}H_{32}MnN_2O_2P_3$: C, 66.68; H, 4.48; N, 3.89. Found: C, 65.44; H, 4.95; N, 3.97. Complex **3** is extremely air sensitive when removed from an inert atmosphere. The low C value can be explained through the oxidation of the NHP phosphorus atom during the shipping/handling process (e.g. $C_{40}H_{32}MnN_2O_3P_3$: C, 65.23; H, 4.38; N, 3.80).

(PP^HP)Mn(CO)$_2$H (4). Complex **3** (49.8 mg, 0.069 mmol) was dissolved in THF (12 mL) and added to a stirring solution of NH_3BH_3 (2.1 mg, 0.068 mmol) dissolved in THF (4 mL). The orange solution gradually lightened to a pale-yellow color and was stirred at room temperature for 12 h. At the end of the reaction, the pale-yellow solution was slightly cloudy. The reaction mixture was filtered through Celite, and the solvent was removed from the filtrate *in vacuo*. The remaining pale-yellow solid was then washed with hexanes (5 × 2 mL), extracted with C_6H_6 (16 mL), and filtered through glass microfiber filter paper. The solvent was removed from the filtrate *in vacuo* to yield **4** in a 2:1 mixture of **4^{syn}** and **4^{anti}** as an off-white powder (44.0 mg, 88%). ^{1}H NMR for **4^{syn}** (600 MHz, C_6D_6): δ 8.02 (m, Ar-H, 4H), 7.77-7.71 (m overlapping with **4^{anti}** signal, Ar-H, 4H), 7.48 (br dd, P^{NHP}-H, $^1J_{H\text{-}PNHP}$ = 372 Hz, $^3J_{H\text{-}H}$ = 14 Hz, 1H), 7.14-6.95 (m overlapping signals and with **4^{anti}** signals, Ar-H, 16H), 6.61-6.57 (m overlapping with **4^{anti}** signal, Ar-H, 2H), 6.50-6.47 (m, Ar-H, 2H), 2.97 (m, CH_2CH_2, 2H), 2.59 (m, CH_2CH_2, 2H), -7.81 (ddt, Mn-H, $^2J_{H\text{-}PNHP}$ = 61 Hz, $^2J_{H\text{-}PPh2}$ = 35 Hz, $^3J_{H\text{-}H}$ = 14 Hz, 1H). ^{1}H NMR for **4^{anti}** (600 MHz, C_6D_6): δ 7.89 (m, Ar-H, 4H), 7.77-7.71 (m overlapping with **4^{syn}** signal, Ar-H, 4H), 7.28 (br dd, P^{NHP}-H, $^1J_{H\text{-}PNHP}$ = 327 Hz, $^3J_{H\text{-}H}$ = 14 Hz, 1H), 7.14-6.95 (m overlapping signals and with **4^{syn}** signals, Ar-H, 16H), 6.61-6.57 (m overlapping with **4^{syn}** signal, Ar-H, 2H), 6.46-6.43 (m, Ar-H, 2H), 2.83 (m, CH_2CH_2, 2H), 2.73 (m, CH_2CH_2, 2H), -7.65 (dt, Mn-H, $^2J_{H\text{-}PPh2}$ = 48 Hz, $^2J_{H\text{-}PNHP}$ = 47 Hz, 1H). ^{1}H NMR for **4^{syn}** (700 MHz, THF-d_8): δ 7.70-7.67 (m, Ar-H, 4H), 7.43-7.29 (m overlapping signals and with **4^{anti}** signals, Ar-H, 14H), 7.28-7.26 (m, Ar-H, 2H), 7.16 (br dd, P^{NHP}-H, $^1J_{H\text{-}P}$ = 373 Hz, $^3J_{H\text{-}H}$ = 13 Hz, 1H), 7.01-6.98 (m, Ar-H, 2H), 6.72-6.69 (m, Ar-H, 2H), 6.65-6.61 (m, Ar-H, 2H), 3.90 (m, CH_2CH_2, 2H), 3.52 (m, CH_2CH_2, 2H), -8.39 (ddt, $^2J_{H\text{-}PNHP}$ = 61 Hz, $^2J_{H\text{-}PPh2}$ = 36 Hz, $^3J_{H\text{-}H}$ = 14 Hz, 1H). ^{1}H NMR for **4^{anti}** (700 MHz, THF-d_8): δ 7.56-7.52 (m, Ar-H, 4H), 7.42-7.39 (m, Ar-H, 4H), 7.34-7.29 (m overlapping signals and with **4^{syn}** signals, Ar-H, 14H), 7.13 (br d, P^{NHP}-H, $^1J_{H\text{-}P}$ = 325 Hz, 1H), 6.97-6.94 (m, Ar-H, 2H), 6.80-6.77 (m, Ar-H, 2H), 6.76-6.73 (m, Ar-H, 2H), 3.61 (m, CH_2CH_2, 2H), 3.56 (m, CH_2CH_2, 2H), -8.19 (dt, $^2J_{H\text{-}PNHP}$ = 46 Hz, $^2J_{H\text{-}PPh2}$ = 47 Hz, 1H). ^{31}P{^{1}H} NMR for **4^{syn}** (242.9 MHz, C_6D_6): δ 156.0 (t, P^{NHP}, $^2J_{P\text{-}PPh2}$ = 85 Hz, 1P), 72.9 (d, PPh_2, $^2J_{P\text{-}PNHP}$ = 85 Hz, 2P). ^{31}P{^{1}H} NMR for **4^{anti}** (242.9 MHz, C_6D_6): δ 157.8 (t, P^{NHP}, $^2J_{P\text{-}PPh2}$ = 85 Hz, 1P), 72.2 (d, PPh_2, $^2J_{P\text{-}PNHP}$ = 86 Hz, 2P). ^{31}P NMR for **4^{syn}** (242.9 MHz, C_6D_6): δ 156.0 (ddt, P^{NHP}, $^1J_{P\text{-}H}$ = 375 Hz, $^2J_{P\text{-}PPh2}$ = 85 Hz, $^2J_{P\text{-}MnH}$ = 63 Hz, 1P), 72.9 (dd, PPh_2, $^2J_{P\text{-}PNHP}$ = 85 Hz, $^2J_{P\text{-}MnH}$ = 33 Hz, 2P). ^{31}P NMR for **4^{anti}** (242.9 MHz, C_6D_6): δ 157.8 (ddt, P^{NHP}, $^1J_{P\text{-}H}$ = 329 Hz, $^2J_{P\text{-}PPh2}$ = 85 Hz, $^2J_{P\text{-}MnH}$ = 48 Hz, 1P), 72.2 (dd, PPh_2, $^2J_{P\text{-}PNHP}$ = 85 Hz, $^2J_{P\text{-}MnH}$ = 48 Hz, 2P). ^{13}C{^{1}H} NMR for **4^{syn}** (176.0 MHz, THF-d_8): δ 226.9 (m, CO), 221.7 (m, CO), 149.1 (m, *ipso*), 139.3 (br d, *ipso*, J = 32 Hz), 138.8 (br d, *ipso*, J = 43 Hz), 134.2 (m), 133.6 (m), 131.9 (s), 131.7 (s), 129.9 (s), 129.6 (s), 128.5 (m), 128.4 (m), 122.3 (br d, *ipso*, J = 48 Hz), 119.8 (s), 115.9 (s), 48.2 (s, CH_2CH_2). ^{13}C{^{1}H} NMR for **4^{anti}** (176.0 MHz, THF-d_8): δ 226.2 (m, CO), 224.5 (m, CO), 148.2 (m, *ipso*), 140.6 (br d, *ipso*, J = 41 Hz), 139.5 (br d, *ipso*, J = 37 Hz), 133.8 (m), 133.6 (m), 133.4 (s), 133.3 (s), 129.6 (s), 129.5 (s), 128.5 (m), 128.2 (m), 124.2 (br d, *ipso*, J = 47 Hz), 120.0 (s), 116.6 (s), 48.0 (s, CH_2CH_2). IR (ATR): 2205 cm^{-1} (νPH), 1938 cm^{-1} (νCO), 1871 cm^{-1} (νCO). Owing to the reactivity of **4** with air and moisture, repeated attempts to acquire satisfactory elemental analysis data were unsuccessful.

(PP^DP)Mn(CO)$_2$D (4-d_2). **4-d_2** was synthesized via an analogous procedure to **4** using ND_3BD_3. Complex **3** (17.0 mg, 0.024 mmol) was dissolved in THF (6 mL) and added to a stirring solution of ND_3BD_3 (2.6 mg, 0.070 mmol) dissolved in THF (4 mL). The orange solution gradually lightened to a pale-yellow color and was stirred at room temperature for 12 h. At the end of the reaction, the pale-yellow solution was slightly cloudy. The reaction mixture was filtered through Celite, and the solvent was removed from the filtrate *in vacuo*. The remaining pale-yellow solid was then washed with hexanes (7 × 2 mL), extracted with C_6H_6 (4 mL), and filtered through glass microfiber filter paper. The solvent was removed from the filtrate *in vacuo* to yield **4-d_2** in a 2:1 mixture of **4^{syn}-d_2** and **4^{anti}-d_2** as an off-white powder (15.5 mg, 91%). Spectroscopic data of **4-d_2** were nearly identical to those of **4** except for the absence of the P^{NHP}-H and Mn-H resonances. ^{1}H NMR for **4^{syn}-d_2** (600 MHz, C_6D_6): δ 8.02 (m, Ar-H, 4H), 7.78-7.71 (m overlapping with **4^{anti}-d_2** signal, Ar-H, 4H), 7.14-6.95 (m overlapping signals and with **4^{anti}-d_2** signals, Ar-H, 16H), 6.62-6.56 (m overlapping

with **4^{anti}-d_2** signal, Ar-H, 2H), 6.50-6.47 (m, Ar-H, 2H), 2.99 (m, CH_2CH_2, 2H), 2.59 (m, CH_2CH_2, 2H). ^{1}H NMR for **4^{anti}-d_2** (600 MHz, C_6D_6): δ 7.89 (m, Ar-H, 4H), 7.78-7.71 (m overlapping with **4^{syn}-d_2** signal, Ar-H, 4H), 7.14-6.95 (m overlapping signals and with **4^{syn}-d_2** signals, Ar-H, 16H), 6.62-6.56 (m overlapping with **4^{syn}-d_2** signal, Ar-H, 2H), 6.46-6.43 (m, Ar-H, 2H), 2.84 (m, CH_2CH_2, 2H), 2.73 (m, CH_2CH_2, 2H). ^{2}H NMR for **4^{syn}-d_2** (92.1 MHz, C_6H_6): δ 7.48 (br d, P^{NHP}-D, $^1J_{D\text{-}P}$ = 371 Hz, 1D), -7.51-(-8.06) (m overlapping with **4^{anti}-d_2** signal, Mn-D, 1D). ^{2}H NMR for **4^{anti}-d_2** (92.1 MHz, C_6H_6): δ 7.28 (br d, P^{NHP}-D, $^1J_{D\text{-}P}$ = 325 Hz, 1D), -7.51-(-8.06) (m overlapping with **4^{syn}-d_2** signal, Mn-D, 1D). ^{2}H NMR for **4^{syn}-d_2** (92.1 MHz, THF): δ 7.19 (br d, P^{NHP}-D, $^1J_{D\text{-}P}$ = 375 Hz, 1D), -8.40 (m, Mn-D, 1D). ^{2}H NMR for **4^{anti}-d_2** (92.1 MHz, THF): δ 7.17 (br d, P^{NHP}-D, $^1J_{D\text{-}P}$ = 330 Hz, 1D), -8.19 (m, Mn-D, 1D). ^{31}P{^{1}H} NMR for **4^{syn}-d_2** (242.9 MHz, C_6D_6): δ 156.3 (m, P^{NHP}, 1P), 73.8 (d, PPh_2, $^2J_{P\text{-}PNHP}$ = 84 Hz, 2P). ^{31}P{^{1}H} NMR for **4^{anti}-d_2** (242.9 MHz, C_6D_6): δ 158.1 (m, P^{NHP}, 1P), 73.0 (d, PPh_2, $^2J_{P\text{-}PNHP}$ = 85 Hz, 2P). ^{31}P NMR or **4^{syn}-d_2** (242.9 MHz, C_6D_6): δ 156.0 (m, P^{NHP}, 1P), 73.8 (d, PPh_2, $^2J_{P\text{-}PNHP}$ = 86 Hz, 2P). ^{31}P NMR for **4^{anti}-d_2** (242.9 MHz, C_6D_6): δ 157.7 (m, P^{NHP}, 1P), 73.0 (d, PPh_2, $^2J_{P\text{-}PNHP}$ = 87 Hz, 2P). IR (ATR): 1939 cm^{-1} (νCO), 1867 cm^{-1} (νCO), 1609 cm^{-1} (νPD).

($PP^{Cl}P$)Mn(CO)$_2$H (5). To a stirring solution of **3** (14.6 mg, 0.020 mmol) dissolved in THF (6 mL) was added a solution of HCl (2.0 M in Et_2O, 20.3 µL, 0.041 mmol) via a glass syringe. The orange solution immediately turned bright yellow and was stirred at room temperature for 2 h. The solvent was removed from the reaction mixture *in vacuo*, and the remaining yellow solid was extracted with C_6H_6 (3 mL) and filtered through Celite. The solvent was then removed *in vacuo* to yield **5** as a yellow powder (10.8 mg, 70%). ^{1}H NMR (600 MHz, C_6D_6): δ 7.92 (m, Ar-H, 4H), 7.75 (m, Ar-H, 4H), 7.20 (m, Ar-H, 2H), 7.11 (m, Ar-H, 4H), 7.10-7.02 (m overlapping signals, Ar-H, 8H), 7.01-6.96 (m overlapping signals, Ar-H, 4H), 6.63 (m, Ar-H, 2H), 3.43 (br s, CH_2CH_2, 2H), 2.82 (br s, CH_2CH_2, 2H), -8.06 (dt, Mn-H, $^2J_{H\text{-}PNHP}$ = 50 Hz, $^2J_{H\text{-}PPh2}$ = 43 Hz, 1H). ^{31}P{^{1}H} NMR (242.9 MHz, C_6D_6): δ 182.9 (t, P^{NHP}, $^2J_{P\text{-}PPh2}$ = 91 Hz, 1P), 70.6 (d, PPh_2, $^2J_{P\text{-}PNHP}$ = 91 Hz, 2P). ^{31}P NMR (242.9 MHz, C_6D_6): δ 182.9 (dt, P^{NHP}, $^2J_{P\text{-}H}$ = 50 Hz, $^2J_{P\text{-}PPh2}$ = 90 Hz, 1P), 70.6 (dd, PPh_2, $^2J_{P\text{-}PNHP}$ = 90 Hz, $^2J_{P\text{-}H}$ = 43 Hz, 2P). ^{13}C{^{1}H} NMR (159.0 MHz, C_6D_6): δ 226.1 (m, CO), 222.9 (m, CO), 146.5 (m, *ipso*), 141.3 (br d, *ipso*, *J* = 45 Hz), 138.1 (br d, *ipso*, *J* = 40 Hz), 135.0 (s), 133.7 (s), 133.2 (s), 131.5 (s), 129.5 (s), 129.4 (s), 128.6 (s), 128.3 (s), 122.3 (br d, *ipso*, *J* = 42 Hz), 121.7 (s), 117.5 (s), 45.3 (s, CH_2CH_2). IR (ATR): 1947 cm^{-1}, 1891 cm^{-1}. Anal. Calcd. for $C_{40}H_{33}MnN_2O_2P_3Cl$: C, 63.46; H, 4.39; N, 3.70. Found: C, 63.44; H, 4.87; N, 3.27.

K(THF)$_2$[(PP^HP)Mn(CO)$_2$] (6). To a stirring solution of **3** (23.6 mg, 0.033 mmol) dissolved in THF (4 mL) was added a solution of $KBEt_3H$ (1.0 M in THF, 65 µL, 0.065 mmol) via a glass syringe. The orange solution immediately turned dark orange-red and was stirred at room temperature for 1 h. The solvent and volatiles were then removed from the reaction mixture *in vacuo*. The remaining dark orange solid was washed with C_6H_6 (4 mL) and room temperature THF (4 mL), then extracted with warm (40 °C) THF (6 mL) and filtered through Celite. The solvent was removed *in vacuo* to afford a crude sample of **6** as a deep orange solid (12.1 mg, 49%). Compound **6** was found to degrade in solution over the course of a few hours. Due to the thermal instability and poor solubility of **6**, the compound could not be isolated in pure form and ^{13}C{^{1}H} NMR and elemental analysis data could not be obtained. However, sufficient characterization data (^{1}H and ^{31}P NMR) is reported. ^{1}H NMR (600 MHz, THF-d_8): δ 7.84 (m, Ar-H, 4H), 7.77 (m, Ar-H, 4H), 7.70 (br d, P^{NHP}-H, $^1J_{H\text{-}P}$ = 362 Hz, 1H), 7.27-7.14 (m overlapping signals, Ar-H, 12H), 7.07 (m, Ar-H, 2H), 6.94 (m, Ar-H, 2H), 6.73-6.70 (m, Ar-H, 2H), 6.51 (m, Ar-H, 2H), 3.80 (m, CH_2CH_2, 2H), 3.62 (m, 2THF, 8H), 3.36 (m, CH_2CH_2, 2H), 1.77 (m, 2THF, 8H). ^{31}P{^{1}H} NMR (242.9 MHz, THF-d_8): δ 142.2 (t, P^{NHP}, $^2J_{P\text{-}PPh2}$ = 117 Hz, 1P), 90.0 (d, PPh_2, $^2J_{P\text{-}PNHP}$ = 117 Hz, 2P). ^{31}P NMR (242.9 MHz, THF-d_8): δ 142.3 (dt, P^{NHP}, $^1J_{P\text{-}H}$ = 362 Hz, $^2J_{P\text{-}PPh2}$ = 117 Hz, 1P), 90.0 (d, PPh_2, $^2J_{P\text{-}PNHP}$ = 117 Hz, 2P). IR (ATR): 1762 cm^{-1} (νCO), 1701 cm^{-1} (νCO).

X-ray Crystallography Procedures. Single-crystal X-ray diffraction studies were carried out on a Bruker Kappa Photon II CPAD diffractometer equipped with Mo Kα radiation (λ = 0.71073 Å) or Cu Kα radiation (λ = 1.54178 Å). Data were collected in a nitrogen gas stream at 100(2) K (Oxford Cryosystems Crysostream 700) using φ and ω scans. The data were integrated using the Bruker SAINT software program and scaled using the SADABS software program within the APEX4 GUI.[63] Solution by dual-space method (SHELXT) produced a complete phasing model for refinement.[64] Refinement was performed within the OLEX2[65] GUI using SHELXL.[66] All nonhydrogen atoms were refined anisotropically by full-matrix least-squares (SHELXL).[66] All hydrogen atoms were placed using a riding model. Their positions were constrained relative to their parent atom using the appropriate FTIX command in SHELXL. Due to unmodelable solvent disorder in the data for **2**, OLEX2 solvent mask was used to remove the electron density from the lattice due to the disordered solvent (CH_2Cl_2) contribution. Publication figures were generated with Mercury.[67] Crystallographic details are summarized in Table S1 of the Supporting Information.

Electrochemistry. Cyclic voltammetry measurements were carried out in a glovebox under a dinitrogen atmosphere in a one-compartment cell using a CH Instruments electrochemical analyzer. A glassy carbon electrode and platinum wire were used as the working and auxiliary electrodes, respectively. The reference electrode was $Ag/AgNO_3$ in THF. Solutions of electrolyte (0.10 M [^{n}Bu$_4$N][PF_6] in THF) and analyte (ca. 2 mM in THF) were also prepared in the glovebox.

Computational Details. All calculations were performed using Gaussian16 for the Linux operating system.[68] DFT calculations were carried out using the M06 functional.[69] A mixed basis set was employed, using the LANL2DZ(*p,d*) double-ζ basis set with effective core potentials for Mn, P, Cl, and Br atoms[70–73] and Gaussian16's internal LANL2DZ basis (equivalent to D95V) for C, H, N, and O atoms.[74] This basis set and functional combination was chosen based on a previous investigation of eight different functional and basis set combinations using related (PPP)Co systems and choosing the combination that attained an optimized geometry closest to the X-ray-derived experimental geometry (M-P distances) while minimizing computational resources.[75] Starting from crystallographically determined coordinates, the geometries of **2** and **3** were optimized to a minimum. The geometries of the theoretical halide exchange products (($PP^{Cl}P$)Mn(CO)$_2$Cl, ($PP^{Br}P$)Mn(CO)$_2$Cl, ($PP^{Br}P$)Mn(CO)$_2$Br) of **2**, stereoisomers (where the Mn-Br bond is either cis or trans to the P-Cl bond) of **2**, and stereoisomers (where the Mn-H bond is cis to the P-H bond (**4^{syn}**), trans to the P-H bond (**4^{anti}**), or trans to the central phosphorus atom (**4^{trans}**)) of **4** were optimized to a minimum from the crystallographically determined coordinates of **2** after editing the necessary atoms in GaussView. Subsequent frequency calculations were carried out to confirm the absence of imaginary frequencies and/or to simulate predicted IR spectra. To find an additional energetic minimum of **3**, the P1-Mn1-C1 angle of 145.45° determined in the optimized distorted square pyramidal structure of **3** (Tables S11-S12) was decreased in 5° increments for eight steps in a modredundant optimization, collecting a relaxed potential energy surface scan and optimizing each geometry. A minimum was found on step four, representing a distorted trigonal bipyramidal geometry. XYZ coordinates of optimized geometries are provided in Tables S4-S9, S11, S14, and S17-S19 of the Supporting Information. NBO[76] calculations were then performed on the optimized geometry of **3** provided in Table S13 of the Supporting Information.

ASSOCIATED CONTENT

Supporting Information

The Supporting Information is available free of charge on the ACS Publications website.

Crystallographic data, DFT calculation results, XYZ coordinates for optimized structures, spectroscopic data for **2**-**6** (PDF).

Accession Codes

CCDC 2260046-2260047 contain the supplementary crystallographic data for this paper. These data can be obtained free of charge via www.ccdc.cam.ac.uk/data_request/cif, or by emailing data_request@ccdc.cam.ac.uk, or by contacting The Cambridge Crystallographic Data Centre, 12 Union Road, Cambridge CB2 1EZ, UK; fax: +44 1223 336033.

AUTHOR INFORMATION

Corresponding Author

Christine M. Thomas – Department of Chemistry and Biochemistry, The Ohio State University, Columbus, Ohio 43210, United States; orcid.org/0000-0001-5009-0479; Email: thomasc@chemistry.ohio-state.edu*

Notes

The authors declare no competing financial interest.

ACKNOWLEDGMENT

This material is based upon work supported by the National Science Foundation under Grant CHE-2101002. The Ohio State University Department of Chemistry and Biochemistry and The Ohio State University Sustainability Institute are gratefully acknowledged for financial support. The authors thank Jeremiah E. Stevens for their help in collecting 700 MHz NMR spectroscopic data.

REFERENCES

(1) Bullock, R. M. *Catalysis without Precious Metals*. Wiley-VCH: Weinheim, 2010.

(2) Chirik, P.; Morris, R. Getting Down to Earth: The Renaissance of Catalysis with Abundant Metals. *Acc. Chem. Res.* **2015**, *48* (9), 2495-2495.

(3) Ludwig, J. R.; Schindler, C. S. Catalyst: Sustainable Catalysis. *Chem 2* **2017**, *2* (3), 313–316.

(4) Nuss, P.; Eckelman, M. J. Life Cycle Assessment of Metals: A Scientific Synthesis. *PLoS One* **2014**, *9* (7), 1–12.

(5) Vesborg, P. C. K.; Jaramillo, T. F. Addressing the Terawatt Challenge: Scalability in the Supply of Chemical Elements for Renewable Energy. *RSC Adv.* **2012**, *2*, 7933–7947.

(6) Alig, L.; Fritz, M.; Schneider, S. First-Row Transition Metal (De)Hydrogenation Catalysis Based on Functional Pincer Ligands. *Chem. Rev.* **2019**, *119* (4), 2681–2751.

(7) Mukherjee, A.; Milstein, D. Homogeneous Catalysis by Cobalt and Manganese Pincer Complexes. *ACS Catal.* **2018**, *8* (12), 11435–11469.

(8) Das, K.; Waiba, S.; Jana, A.; Maji, B. Manganese-Catalyzed Hydrogenation, Dehydrogenation, and Hydroelementation Reactions. *Chem. Soc. Rev.* **2022**, *51*, 4386–4464.

(9) Mukherjee, A.; Nerush, A.; Leitus, G.; Shimon, L. J. W.; Ben David, Y.; Espinosa Jalapa, N. A.; Milstein, D. Manganese-Catalyzed Environmentally Benign Dehydrogenative Coupling of Alcohols and Amines to Form Aldimines and H_2: A Catalytic and Mechanistic Study. *J. Am. Chem. Soc.* **2016**, *128* (13), 4298–4301.

(10) Mastalir, M.; Glatz, M.; Gorgas, N.; Stöger, B.; Pittenauer, E.; Allmaier, G.; Veiros, L. F.; Kirchner, K. Divergent Coupling of Alcohols and Amines Catalyzed by Isoelectronic Hydride Mn^{I} and Fe^{II} PNP Pincer Complexes. *Chem. Eur. J.* **2016**, *22*, 12316–12320.

(11) Kumar, A.; Espinosa-Jalapa, N. A.; Leitus, G.; Diskin-Posner, Y.; Avram, L.; Milstein, D. Direct Synthesis of Amides by Dehydrogenative Coupling of Amines with Either Alcohols or Esters: Manganese Pincer Complex as Catalyst. *Angew. Chem. Int. Ed.* **2017**, *56*, 14992–14996.

(12) Kallmeier, F.; Dudziec, B.; Irrgang, T.; Kempe, R. Manganese-Catalyzed Sustainable Synthesis of Pyrroles from Alcohols and Amino Alcohols. *Angew. Chem. Int. Ed.* **2017**, *56*, 7261–7265.

(13) Borghs, J. C.; Lebedev, Y.; Rueping, M.; El-Sepelgy, O. Sustainable Manganese-Catalyzed Solvent-Free Synthesis of Pyrroles from 1,4-Diols and Primary Amines. *Org. Lett.* **2019**, *21* (1), 70–74.

(14) Mastalir, M.; Glatz, M.; Pittenauer, E.; Allmaier, G.; Kirchner, K. Sustainable Synthesis of Quinolines and Pyrimidines Catalyzed by Manganese PNP Pincer Complexes. *J. Am. Chem. Soc.* **2016**, *138* (48), 15543–15546.

(15) Mondal, A.; Sahoo, M. K.; Subaramanian, M.; Balaraman, E. Manganese(I)-Catalyzed Sustainable Synthesis of Quinoxaline and Quinazoline Derivatives with the Liberation of Dihydrogen. *J. Org. Chem.* **2020**, *85* (11), 7181–7191.

(16) Deibl, N.; Kempe, R. Manganese-Catalyzed Multicomponent Synthesis of Pyrimidines from Alcohols and Amidines. *Angew. Chem. Int. Ed.* **2017**, *56*, 1663–1666.

(17) Bertini, F.; Glatz, M.; Gorgas, N.; Stöger, B.; Peruzzini, M.; Veiros, L. F.; Kirchner, K.; Gonsalvi, L. Carbon Dioxide Hydrogenation Catalysed by Well-Defined Mn(I) PNP Pincer Hydride Complexes. *Chem. Sci.* **2017**, *8*, 5024–5029.

(18) Kar, S.; Goeppert, A.; Kothandaraman, J.; Prakash, G. K. S. Manganese-Catalyzed Sequential Hydrogenation of CO_2 to Methanol via Formamide. *ACS Catal.* **2017**, *7* (9), 6347–6351.

(19) Kostera, S.; Weber, S.; Peruzzini, M.; Veiros, L. F.; Kirchner, K.; Gonsalvi, L. Carbon Dioxide Hydrogenation to Formate Catalyzed by a Bench-Stable, Non-Pincer-Type Mn(I) Alkylcarbonyl Complex. *Organometallics* **2021**, *40* (9), 1213–1220.

(20) Hert, C. M.; Curley, J. B.; Kelley, S. P.; Hazari, N.; Bernskoetter, W. H. Comparative CO_2 Hydrogenation Catalysis with MACHO-Type Manganese Complexes. *Organometallics* **2022**, *41* (22), 3332–3340.

(21) Peris, E.; Crabtree, R. H. Key Factors in Pincer Ligand Design. *Chem. Soc. Rev.* **2018**, *47*, 1959–1968.

(22) Elangovan, S.; Topf, C.; Fischer, S.; Jiao, H.; Spannenberg, A.; Baumann, W.; Ludwig, R.; Junge, K.; Beller, M. Selective Catalytic Hydrogenations of Nitriles, Ketones, and Aldehydes by Well-Defined Manganese Pincer Complexes. *J. Am. Chem. Soc.* **2016**, *138*, 8809–8814.

(23) Kallmeier, F.; Irrgang, T.; Dietel, T.; Kempe, R. Highly Active and Selective Manganese C=O Bond Hydrogenation Catalysts: The Importance of the Multidentate Ligand, the Ancillary Ligands, and the Oxidation State. *Angew. Chem. Int. Ed.* **2016**, *55*, 11806–11809.

(24) Freitag, F.; Irrgang, T.; Kempe, R. Mechanistic Studies of Hydride Transfer to Imines from a Highly Active and Chemoselective Manganate Catalyst. *J. Am. Chem. Soc.* **2019**, *141* (29), 11677–11685.

(25) Wang, Y.; Liu, S.; Yang, H.; Li, H.; Lan, Y.; Liu, Q. Structure, Reactivity and Catalytic Properties of Manganese-Hydride Amidate Complexes. *Nat. Chem.* **2022**, *14*, 1233–1241.

(26) Khusnutdinova, J. R.; Milstein, D. Metal-Ligand Cooperation. *Angew. Chem. Int. Ed.* **2015**, *54* (42), 12236–12273.

(27) Wang, Y.; Zhu, L.; Shao, Z.; Li, G.; Lan, Y.; Liu, Q. Unmasking the Ligand Effect in Manganese-Catalyzed Hydrogenation: Mechanistic Insight and Catalytic Application. *J. Am. Chem. Soc.* **2019**, *141* (43), 17337–17349.

(28) Abhyankar, P.; Macmillan, S. N.; Lacy, D. C. Activation of H_2 with Dinuclear Manganese(I)-Phosphido Complexes. *Organometallics* **2022**, *41* (1), 60–66.

(29) Abhyankar, P. C.; Macmillan, S. N.; Lacy, D. C. Bench-Stable Dinuclear Mn(I) Catalysts in *E*-Selective Alkyne Semihydrogenation: A Mechanistic Investigation. *Chem. Eur. J.* **2022**, *28*, e202201766.

(30) Gediga, M.; Feil, C. M.; Schlindwein, S. H.; Bender, J.; Nieger, M.; Gudat, D. N-Heterocyclic Phosphenium Complex of Manganese: Synthesis and Catalytic Activity in Ammonia Borane Dehydrogenation. *Chem. Eur. J.* **2017**, *23* (48), 11560–11569.

(31) Gediga, M.; Schlindwein, S. H.; Bender, J.; Nieger, M.; Gudat, D. Variable Reactivity of a N-Heterocyclic Phosphenium Complex: P-C Bond Activation or "Abnormal" Deprotonation. *Angew. Chem. Int. Ed.* **2017**, *56*, 15718–15722.

(32) Day, G. S.; Pan, B.; Kellenberger, D. L.; Foxman, B. M.; Thomas, C. M. Guilty as Charged: Non-Innocent Behavior by a Pincer Ligand Featuring a Central Cationic Phosphenium Donor. *Chem. Commun.* **2011**, *47* (12), 3634–3636.

(33) Poitras, A. M.; Bezpalko, M. W.; Foxman, B. M.; Thomas, C. M. Cooperative Activation of O-H and S-H Bonds Across the Co-P Bond of an N-Heterocyclic Phosphido Complex. *Dalton Trans.* **2019**, *48* (9), 3074–3079.

(34) Poitras, A. M.; Knight, S. E.; Bezpalko, M. W.; Foxman, B. M.; Thomas, C. M. Addition of H_2 Across a Cobalt–Phosphorus Bond. *Angew. Chem. Int. Ed.* **2018**, *57* (6), 1497–1500.

(35) Poitras, A. M.; Oliemuller, L. K.; Hatzis, G. P.; Thomas, C. M. Highly Selective Hydroboration of Terminal Alkenes Catalyzed by a Cobalt Pincer Complex Featuring a Central Reactive N-Heterocyclic Phosphido Fragment. *Organometallics* **2021**, *40* (8), 1025–1031.

(36) Pan, B.; Bezpalko, M. W.; Foxman, B. M.; Thomas, C. M. Heterolytic Addition of E-H Bonds across Pt-P Bonds in Pt *N*-Heterocyclic Phosphenium/Phosphido Complexes. *Dalton Trans.* **2012**, *41* (30), 9083–9090.

(37) Hatzis, G. P.; Oliemuller, L. K.; Dickie, D. A.; Thomas, C. M. N-Heterocyclic Phosphido Complexes of Rhodium Supported by a Rigid Pincer Ligand. *Eur. J. Inorg. Chem.* **2020**, 2873–2881.

(38) Oliemuller, L. K.; Moore, C. E.; Thomas, C. M. Electronic and Structural Variations of a Nickel(0) N-Heterocyclic Phosphenium Complex in Comparison to Group 10 Analogues. *Inorg. Chem.* **2022**, *61*, 19440–19451.

(39) Rosenberg, L. Metal Complexes of Planar PR_2 Ligands: Examining the Carbene Analogy. *Coord. Chem. Rev.* **2012**, *256* (5–8), 606–626.

(40) Weber, S.; Stöger, B.; Kirchner, K. Hydrogenation of Nitriles and Ketones Catalyzed by an Air-Stable Bisphosphine Mn(I) Complex. *Org. Lett.* **2018**, *20*, 7212–7215.

(41) Cowley, A. H.; Kemp, R. A. Synthesis and Reaction Chemistry of Stable Two-Coordinate Phosphorus Cations (Phosphenium Ions). *Chem. Rev.* **1985**, *85* (5), 367–382.

(42) Tondreau, A. M.; Boncella, J. M. 1,2-Addition of Formic or Oxalic Acid to $^-N\{CH_2CH_2(PiPr_2)\}_2$-Supported Mn(I) Dicarbonyl Complexes and the Manganese-Mediated Decomposition of Formic Acid. *Organometallics* **2016**, *35*, 2049–2052.

(43) P Pan, B.; Xu, Z.; Bezpalko, M. W.; Foxman, B. M.; Thomas, C. M. N-Heterocyclic Phosphenium Ligands as Sterically and Electronically-Tunable Isolobal Analogues of Nitrosyls. *Inorg. Chem.* **2012**, *51* (7), 4170–4179.

(44) Evers-McGregor, D. A.; Bezpalko, M. W.; Foxman, B. M.; Thomas, C. M. N-Heterocyclic Phosphenium and Phosphido Nickel Complexes Supported by a Pincer Ligand Framework. *Dalton Trans.* **2016**, *45* (5), 1918–1929.

(45) Addison, A. W.; Rao, T. N.; Reedijk, J.; van Rijn, J.; Verschoor, G. C. Synthesis, Structure, and Spectroscopic Properties of Copper(II) Compounds Containing Nitrogen-Sulphur Donor Ligands; the Crystal and Molecular Structure of Aqua[1,7-bis(*N*-methylbenzimidazol-2'-yl)-2,6-dithiaheptane]copper(II) Perchlorate. *J. Chem. Soc., Dalton Trans.* **1984**, 1349–1356.

(46) Radosevich, A. T.; Melnick, J. G.; Stoian, S. A.; Bacciu, D.; Chen, C.; Foxman, B. M.; Ozerov, O. V; Nocera, D. G. Ligand Reactivity in Diarylamido/Bis(Phosphine) PNP Complexes of $Mn(CO)_3$ and $Re(CO)_3$. *Inorg. Chem.* **2009**, *48*, 9214–9221.

(47) Das, U. K.; Ben-David, Y.; Diskin-Posner, Y.; Milstein, D. N-Substituted Hydrazones by Manganese-Catalyzed Coupling of Alcohols with Hydrazine: Borrowing Hydrogen and Acceptorless Dehydrogenation in One System. *Angew. Chem. Int. Ed.* **2018**, *57*, 2179–2182.

(48) Anderson, N. H.; Boncella, J.; Tondreau, A. M. Manganese-Mediated Formic Acid Dehydrogenation. *Chem. Eur. J.* **2019**, *25*, 10557–10560.

(49) Yang, W.; Chernyshov, I. Yu.; van Schendel, R. K. A.; Weber, M.; Müller, C.; Filonenko, G. A.; Pidko, E. A. Robust and Efficient Hydrogenation of Carbonyl Compounds Catalysed by Mixed Donor Mn(I) Pincer Complexes. *Nat. Commun.* **2021**, *12*, 12.

(50) Gawali, S. S.; Pandia, B. K.; Pal, S.; Gunanathan, C. Manganese(I)-Catalyzed Cross-Coupling of Ketones and Secondary Alcohols with Primary Alcohols. *ACS Omega* **2019**, *4* (6), 10741–10754.

(51) Yang, W.; Chernyshov, I. Yu.; Weber, M.; Pidko, E. A.; Filonenko, G. A. Switching Between Hydrogenation and Olefin Transposition Catalysis via Silencing NH Cooperativity in Mn(I) Pincer Complexes. *ACS Catal.* **2022**, *12* (17), 10818–10825.

(52) Espinosa-Jalapa, N. A.; Nerush, A.; Shimon, L. J. W.; Leitus, G.; Avram, L.; Ben-David, Y.; Milstein, D. Manganese-Catalyzed Hydrogenation of Esters to Alcohols. *Chem. Eur. J.* **2017**, *23*, 5934–5938.

(53) Borghs, J. C.; Tran, M. A.; Sklyaruk, J.; Rueping, M.; El-Sepelgy, O. Sustainable Alkylation of Nitriles with Alcohols by Manganese Catalysis. *J. Org. Chem.* **2019**, *84* (12), 7927–7935.

(54) Staubitz, A.; Robertson, A. P. M.; Manners, I. Ammonia-Borane and Related Compounds as Dihydrogen Sources. *Chem. Rev.* **2010**, *110*, 4079–4124.

(55) Pandey, B.; Krause, J. A.; Guan, H. Iron Dihydride Complex Stabilized by an All-Phosphorus-Based Pincer Ligand and Carbon Monoxide. *Inorg. Chem.* **2022**, *61* (29), 11143–11155.

(56) Heurich, T.; Qu, Z.; Kunzmann, R.; Schnakenburg, G.; Engeser, M.; Nožinović, S.; Streubel, R. Styrene Polymerization under Ambient Conditions by using a Transient 1,3,2-Diazaphospholane-2-oxyl Complex. *Chem. Eur. J.* **2018**, *24*, 6473–6478.

(57) Snow, S. S.; Jiang, D.; Parry, R. W. Preparation of New Bis(dialkylamino)phosphine Species via Redcution of Bis(dialkylamino)halophosphines. *Inorg. Chem.* **1985**, *24*, 1460–1463.

(58) Feil, C. M.; Hettich, T. D.; Beyer, K.; Sondermann, C.; Schlindwein, S. H.; Nieger, M.; Gudat, D. Comparing the Ligand Behavior of N-Heterocyclic Phosphenium and Nitrosyl Units in Iron and Chromium Complexes. *Inorg. Chem.* **2019**, *58*, 6517–6528.

(59) Narro, A. L.; Arman, H. D.; Tonzetich, Z. J. Manganese Chemistry of Anionic Pyrrole-Based Pincer Ligands. *Organometallics* **2019**, *38* (8), 1741–1749.

(60) Pan, Baofei. Late Transition Metal Complexes Containing Tridentate Pincer-Type 1, 3-bis(*o*-(diphenylphosphino)phenyl)-*N*, *N'*-Heterocyclic Phosphenium/Carbene Ligands. Doctor of Philosophy, Brandeis University, Waltham, MA, August 2012.

(61) Ramachandran, P. V.; Gagare, P. D. Preparation of Ammonia Borane in High Yield and Purity, Methanolysis, and Regeneration. *Inorg. Chem.* **2007**, *46*, 7810–7817.

(62) Fulmer, G. R.; Miller, A. J. M.; Sherden, N. H.; Gottlieb, H. E.; Nudelman, A.; Stoltz, B. M.; Bercaw, J. E.; Goldberg, K. I. NMR Chemical Shifts of Trace Impurities: Common Laboratory Solvents, Organics, and Gases in Deuterated Solvents Relevant to the Organometallic Chemist. *Organometallics* **2010**, *29* (29), 2176–2179.

(63) Bruker AXS. *Apex4*; *SAINT*, *v. 8.40b*; *SADABS, v. 2016/2*; Bruker XS, Inc.; Madison, Wisconsin, USA, 2016.

(64) Sheldrick, G. M. SHELXT - Integrated Space-group and Crystal-structure Determination. *Acta Crystallograph., Sect. A: Found. Adv.* **2015**, *71*, 3–8.

(65) Dolomanov, O. V; Bourhis, L. J.; Gildea, R. J.; Howard, J. A. K.; Puschmann, H. OLEX2: A Complete Structure Solution, Refinement, and Analysis Program. *J. Appl. Crystallograph.* **2009**, *42* (2), 339–341.

(66) Sheldrick, G. M. Crystal Structure Refinement with SHELXL. *Acta Crystallograph., Sect. C: Struct. Chem.* **2015**, *71*, 3–8.

(67) Macrae, C. F.; Bruno, I. J.; Chisholm, J. A.; Edgington, P. R.; McCabe, P.; Pidcock, E.; Rodriguez-Monge, L.; Taylor, R.; Van de Streek, J.; Wood, P. A. Merucry CSD 2.0 - New Features for the Visualization and Investigation of Crystal Structures. *J. Appl. Crystallogr.* **2008**, *41* (2), 466–470.

(68) Frisch, M. J.; Trucks, G. W.; Schlegel, H. B.; Scuseria, G. E.; Robb, M. A.; Cheeseman, J. R.; Scalmani, G.; Barone, V.; Petersson, G. A.; Nakatsuji, H.; Li, X.; Caricato, M.; Marenich, A. V.; Bloino, J.; Janesko, B. G.; Gomperts, R.; Mennucci, B.; Hratchian, H. P.; Ortiz, J. V.; Izmaylov, A. F.; Sonnenberg, J. L.; Williams Ding, F.; Lipparini, F.; Egidi, F.; Goings, J.; Peng, B.; Petrone, A.; Henderson, T.; Ranasinghe, D.; Zakrzewski, V. G.; Gao, J.; Rega, N.; Zheng, G.; Liand, W.; Hada, M.; Ehara, M.; Toyota, K.; Fukuda, R.; Hasegawa, J.; Ishida, M.; Nakajima, T.; Honda, Y.; Kitao, O.; Nakai, H.; Vreven, T.; Throssell, K.; Montgomery, J. A., Jr.; Peralta, J. E.; Ogliaro, F.; Bearpark, M. J.; Hyed, J. J.; Brothers, E. N.; Kudin, K. N.; Staroverov, V. N.; Keith, T. A.; Kobayashi, R.; Normand, J.; Raghavachari, K.; Rendell, A. P.; Burant, J. C.; Iyengar, S. S.; Tomasi, J.; Cossi, M.; Millam, J. M.; Klene, M.; Adamo, C.; Cammi, R.; Ochterski, J. W.; Martin, R. L.; Morokuma, K.; Farkas, O.; Foresman, J. B.; Fox, D. J. *Gaussian 16*, rev. C.01; Gaussian, Inc.; Wallingford, CT, 2016.

(69) Zhao, Y.; Truhlar, D. G. The M06 Suite of Density Functionals for Main Group Thermochemistry, Thermochemical Kinetics,

Noncovalent Interactions, Excited States, and Transition Elements: Two New Functionals and Systematic Testing of Four M06-Class Functionals and 12 Other Function. *Theor. Chem. Acc.* **2008**, *120*, 215–241.

(70) Hay, P. J.; Wadt, W. R. *Ab Initio* Effective Core Potentials for Molecular Calculations. Potentials for K to Au Including the Outermost Core Orbitals. *J. Chem. Phys.* **1985**, *82*, 299–310.

(71) Hay, P. J.; Wadt, W. R. *Ab Initio* Effective Core Potentials for Molecular Calculations. Potentials for the Transition-Metal Atoms Sc to Hg. *J. Chem. Phys.* **1985**, *82*, 270–283.

(72) Wadt, W. R.; Hay, P. J. *Ab Initio* Effective Core Potentials for Molecular Calculations. Potentials for Main Group Elements Na to Bi. *J. Chem. Phys.* **1985**, *82*, 284–298.

(73) Roy, L. E.; Hay, P. J.; Martin, R. L. Revised Basis Sets for the LANL Effective Core Potentials. *J. Chem. Theory Comput.* **2008**, *4*, 1029–1031.

(74) Dunning, T. H.; Hay, P. J. *Modern Theoretical Chemistry*; Schaefer, H. F., Ed.; Plenum: New York, 1976; Vol. 3, pp 1-28.

(75) Poitras, A. M.; Bezpalko, M. W.; Moore, C. E.; Dickie, D. A.; Foxman, B. M.; Thomas, C. M. A Series of Dimeric Cobalt Complexes Bridged by N-Heterocyclic Phosphido Ligands. *Inorg. Chem.* **2020**, *59*, 4729–4740.

(76) Glendening, E. D.; Reed, A. E.; Carpenter, J. E.; Weinhold, F. *NBO*, Version 3.1; Gaussian Inc., 2003.

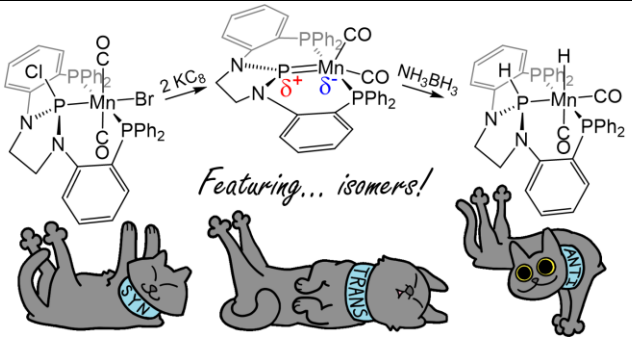

A $(PPP)Mn(CO)_2$ complex of manganese featuring a central three-coordinate N-heterocyclic phosphorus fragment is synthesized and its reactivity towards H_2, NH_3BH_3, H^+, and H^- is explored. Computational methods and reactivity studies are used to assess the electrophilic nature of the N-heterocyclic phosphenium moiety and the nucleophilic manganese center, which contrasts previously reported pincer-ligated dicarbonyl Mn^I species.